Transient Photoluminescence measurement of Perovskite to study Ion Migration

Bachelor Thesis

submitted by

Hein, Franz Sebastian

at the

University of Konstanz

Department of Physics

Prof. Dr. Bruno Ehrler (AMOLF Institute Amsterdam)

Prof. Dr. Lukas Schmidt-Mende (University of Konstanz)

Konstanz

March 1, 2024

Abstract

For over a decade, metal halide perovskites have garnered significant attention due to their excellent photovoltaic properties. These complex semiconductors exhibit a unique interplay of optical, electronic, and ionic effects, presenting uncertainties and challenges yet to be overcome. Most prominently among these challenges, is the migration and accumulation of ions within perovskites, which profoundly impacts various properties.
In this study, the influence of metal electrodes on ion dynamics is investigated using photoluminescence mapping under electrical bias measurements. A comprehensive description of each observed feature is provided, the metals' impact on them is analysed, and mechanistic explanations proposed. Remarkably, among other features, is the emergence of bright fronts characterised by increased luminescence intensity emerging from near the anode. These hardly reported bright fronts are hypothesised to arise from ion-induced changes in the electrical field gradient, leading to local charge density and luminescence signal increases. Alternatively, migrating ions may quench non-radiative recombination by shifting band energies and changing trap occupation states. Based on this and previous work, the main bright feature is ascribed to intrinsic perovskite effects, independent of the metal contacts or transport layer.
Analysis reveals that copper, gold, and silver electrodes all exhibit similar features, albeit with significant variations in their appearance. Silver devices produce intense bright fronts that move faster and extend farther across the channel compared to those with gold or copper electrodes. Moreover, a dark front at the anode on longer timescales, most prevalent for copper devices, and an increase in luminescence intensity at the cathode, strongest for gold devices, are observed.
The study reveals previously underappreciated phenomena related to ion migration, further study of which might deepen our understanding of ion dynamics in general. Additionally, a non-negligible impact of the metal choice is uncovered, prompting reassessment of that interaction.

Zusammenfassung

Seit über einem Jahrzehnt erregen Metallhalogenid-Perovskite aufgrund ihrer ausgezeichneten photovoltaischen Eigenschaften erhebliche Aufmerksamkeit. Diese komplexen Halbleiter sind für ihr Zusammenspiel optischer, elektronischer und ionischer Effekte bekannt. Diese stellen Ungewissheiten und Herausforderungen dar, die noch zu bewältigen sind. Am deutlichsten unter diesen Herausforderungen steht die Migration von Ionen innerhalb der Perowskite, die verschiedene Eigenschaften stark beeinflusst.

In dieser Arbeit wird der Einfluss von Metallelektroden auf die Ionen-Dynamik mittels Photolumineszenz-Messungen unter elektrischer Spannung untersucht. Es wird eine umfassende Beschreibung aller beobachteten Merkmale präsentiert, die Auswirkungen der Metalle darauf werden analysiert und erklärende Mechanismen vorgeschlagen. Bemerkenswert ist unter anderem das Auftreten von hellen Fronten, die sich durch erhöhte Lumineszenzintensität in der Nähe der Anode auszeichnen. Es wird vermutet, dass diese kaum bekannten hellen Fronten aus ioneninduzierten Änderungen des elektrischen Feldes entstehen, was zu lokalen Ladungsdichte- und Lumineszenzsignalerhöhungen führt. Alternativ können migrierende Ionen die nicht-strahlende Rekombination durch Verschiebung der Bandenergien und Änderung der Fallenzustands-Besetzung verringern.

Basierend auf dieser und früheren Arbeiten wird das Hauptmerkmal als intrinsischer Perowskit-Effekt gedacht, der unabhängig von den Metallkontakten oder der Transportchicht auftritt. Die Analyse zeigt, dass Kupfer-, Gold- und Silberelektroden alle grundlegend ähnliche Merkmale aufweisen, wenn auch mit signifikanten Variationen in ihrem Erscheinungsbild. Silbergeräte erzeugen intensive helle Fronten, die sich schneller bewegen und sich weiter über den Kanal erstrecken als solche mit Gold- oder Kupferelektroden. Darüber hinaus werden eine dunkle Front an der Anode über längere Zeiträume, am häufigsten und intensivsten bei Kupfergeräten, und eine Zunahme der Lumineszenzintensität an der Kathode, am stärksten bei Goldgeräten, beobachtet.

Die Studie enthüllt zuvor unerkannte Phänomene im Zusammenhang mit der Ionenmigration, deren weitere Untersuchung unser Verständnis der Ionen-Dynamik im Allgemeinen vertiefen könnte. Darüber hinaus wird ein nicht unerheblicher Einfluss der Metallwahl aufgedeckt, der eine Neubewertung dieser Interaktion veranlasst.

Contents

1 Introduction

With the climate crisis showing its dramatic consequences [1], the urgency of a paradigm shift in energy production and consumption becomes pressingly obvious. On the one hand, the trajectory of escalating energy consumption (fig 1.1) has to be reverted to one of reduction, while on the other hand sustainable energy production has to be omnipresent to achieve the required net-zero greenhouse gas emissions [1]. Addressing this existential challenge demands a multifaceted approach, wherein electricity generation, though pivotal, represents only one of those facets. Although more than 50 % of worldwide electricity generation is made up of fossil fuels [2], a growing share of renewable sources demonstrate due shifts in the sector. Among renewables, solar energy, and particularly photovoltaics (PV), stand out as key emerging contributors to this positive trajectory [3]. Silicon-based solar cells have dominated the commercial PV landscape thus far representing 95 % of the PV market [4], yet other contenders have been gaining momentum in the realm of research. One such contender, a material class known as perovskites, has gained attention over the past 15 years [5]. Despite their promise, the intricacies of metal halide perovskites remain incompletely understood, presenting researchers with ongoing challenges. Among other use cases the goal of establishing commercially viable perovskite solar cells, a low cost, high efficiency, light weight, and solution processable alternative to silicon, is supported by huge investments of resources and research [6].

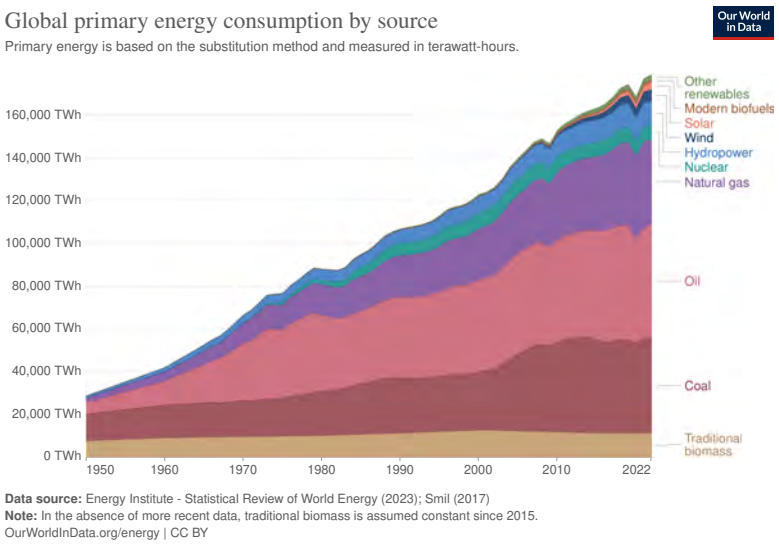

Fig. 1.1: Overview of global energy consumption from the year 1950 to 2022. [3].

Perovskite, its Merits and Liabilities

The Perovskite crystal structure as a material class can be composed of different elements and molecules, but organic-inorganic metal halide perovskites are the specific group of interest in this research project. At its core, metal halide perovskites can be conceptualised as semiconductors with highly favorable attributes for photovoltaics, i.e. the conversion of light to electricity. Most promising among these attributes are its exceptional light absorption capabilities and tunable bandgap, enabling efficient capture of sunlight. Additionally, the low production costs stemming from abundant resources and energy-efficient fabrication processes contribute to its appeal. Furthermore, perovskite's versatility is exemplified by its mechanical flexibility, rendering it compatible with soft substrates. Its great light absorption properties enable the production of thin films, resulting in lightweight structures conducive to widespread installation. Finally, perovskites serve as great wide-bandgap absorber materials for high-efficiency tandem solar cells. [7][8]

However, despite these promising characteristics, common perovskite materials are hindered by significant drawbacks, primarily their instability. While standard silicon solar cells can maintain functionality over decades, certain PSCs (e.g. PSCs based on the prototypical $CH_3NH_3PbI_3$/MAPbI Pervoskite) exhibit substantial degradation within mere days of exposure to light, heat, moisture, and oxygen [9]. The pursuit of commercializing PSCs is impeded by this instability, making it a focal point of perovskite research. Besides the major problem of instability, the sometimes lacking reproducibility of perovskites adds to its liabilities and hinders widespread adoption.
The complex ionic crystal structure and the specific composition its made of play a pivotal role in both the operational mechanisms and degradation processes of PSCs. Of particular importance is the phenomenon of ion migration, wherein certain weakly bonded ions within the crystal lattice are dislocated and migrate through the material. This phenomenon gives rise to a plethora of effects, each deserving of thorough investigation, but it is thought to be the main source of perovskites instability [9]. This research endeavors to investigate some of these effects, contributing to a deeper understanding of PSCs and potentially paving the way for addressing their stability issues.

Research Question and Objectives

Understanding the intricate and complex mechanisms governing perovskites is paramount for the societal viability of PSCs. Consequently, extensive research has been dedicated to probe, characterize, and utilize perovskites unique properties. Investigating the migration and accumulation of ions poses a challenge due to the limited methods available. However, one such method is based on photoluminescence (PL), where the material of interest absorbs photons of a specific energy and subsequently emits photons at a lower energy level. Analysis of the emitted light provides valuable insights into fundamental characteristics such as the bandgap energy. Introducing time resolution to PL provides more information about the processes at hand. There are two separate time regimes of interest; firstly, that of electronic processes in the femto- to milliseconds and secondly, ionic motions in the sub-seconds to minutes. In order to study movements of ions, a bias voltage is applied across the perovskite to force charged ions to drift parallel or anti-parallel to the applied field, depending on the field's polarity and ion charge. These ionic motions influence the PL signal, enabling real-time monitoring of migration and accumulation - a method referred to as Photoluminescence under Bias (PLuB).
The primary objectives of this study are twofold: firstly, to generally study ion dynamics in perovskites and enhance our understanding and secondly, to examine the impact of metal electrodes on these processes.
The second objective of this study, the metal specific impact on ionic motions within the perovskite remains mostly unclear, owing to the intricate relationships between different materials and layers, coupled with a lack of research specifically targeting this interaction.
Utilizing PLuB and complementary methods, an effort is made to clarify the relation between metal, perovskite and ion dynamics, assess to which extend the metal even influences the ion dynamics and theorize mechanisms to explain the observed results. While achieving a comprehensive understanding lies beyond the scope of this work, it aims to lay the groundwork for further research and contribute to unravelling the complexities of dynamic ion behavior in perovskites.

2 Theory

In this section, a brief overview of the key theoretical concepts is provided. To begin with, the perovskite crystal structure is introduced, followed by an examination of ion migration. Subsequently, an introduction to the mechanisms governing junctions, meaning interfaces between different materials or layers, is presented. The devices investigated in this work are then introduced, followed by a discussion of the methods and measurement techniques utilised.

2.1 Perovskite

The name perovskite is derived from the Russian Lev Perovski after whom the naturally occurring mineral $CaTiO_3$ is named [10]. The perovskite structure encompasses all materials that crystallise into the structure of that mineral. However, in this study, the focus is solely on specific organic-inorganic metal halide perovskites due to their characteristics that make them suitable for photovoltaic applications. Therefore, whenever perovskite is mentioned, it refers specifically to the metal halide subclass, not the original mineral.

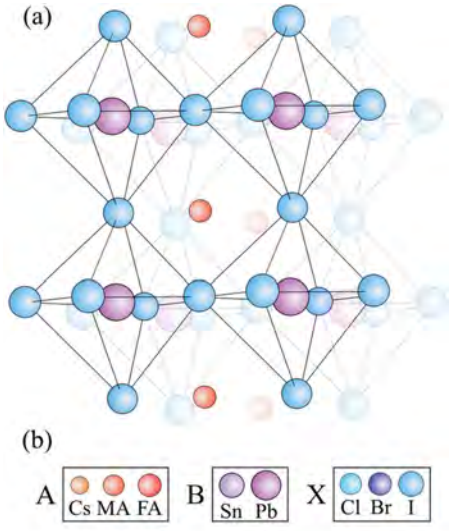

Fig. 2.1: (a) Illustration of the ABX_3 tetragonal perovskite crystal structure. (b) list of common elements or molecules for each site. Adapted from [11].

2.1.1 An Atypical Semiconductor

Perovskite is a semiconductor characterised by ionic chemical bonds between its components, typically comprising a blend of organic molecules and inorganic atoms. The general chemical formula or stoichiometry, ABX_3, consists of a monovalent cation A - commonly methylammonium (MA^+ / $CH_3NH_3^+$), formamidinium (FA^+ / $CH(NH_2)^+$) or Cs^+ - a divalent metal cation B, predominantly Pb^{2+} or occasionally Sn^{2+}, and halide anions X, such as Cl^-, Br^- or I^- [12]. It is common practise to mix different components to tune certain properties of the perovskite to increase performance and stability [13][14]. For instance, in this study, a double cation double halide perovskite $Cs_{0.18}FA_{0.82}$ Pb $I_{2.82}Br_{0.18}$ is used. Within this complex crystal structure, the halides and lead form an octahedron surrounded by the organic cations, wherein the size, composition and other characteristics of the components influence its properties [7]. However, the weak bonding between the BX_3 octahedra and the A cations, among other reasons, results in a soft lattice, facilitating the displacement and movement of ions through the lattice itself [15]. While a soft lattice, shallow trap states, and tunable properties such as the bandgap offer considerable utility, these weak bonds and the ionic movements can also cause inconsistencies and instability. Thus, the remarkable opto-electronic properties entice the commercialisation of PSCs, yet the poorly understood mixed electronic-ionic behaviour impedes their practical implementation.

2.1.2 Ion Dynamics

The focus of this research project centers on the study of ionic motions within a perovskite layer. But how does this behavior manifest and what is the current extent of understanding regarding the various processes and dynamics involved?
While the crystal structure of perovskites has been covered in the previous section under ideal conditions, in reality, perovskites exhibit imperfections and impurities across different scales. These include diverse formations of grains with chaotic boundaries at the macro scale [16], segregated phases or regions of differing stoichiometry [9], as well as microscopic defects like vacancies, antisites, and interstitials[16]. To begin with, it is instructive to look at the micro scale and tackle basic questions like: What are the possible ionic defects, which are most likely to occur, what detrimental effects can they induce, and how can their dynamics be comprehended?
A foundational work by Eames et al., employing both theoretical and experimental techniques, identified ion migration as primarily vacancy-mediated and provided according activation energies (for classic $MAPbI_3$: $E_A(I^-) = 0.58\,\text{eV}$, $E_A(MA^+) = 0.84\,\text{eV}$ and

$E_A(Pb^{2+}) = 2.31\,\text{eV}$) [17]. Despite ongoing debates regarding the precise activation energies, a qualitative summary by Zuo et al. reports that the X halides exhibit the lowest activation energies and are thus most prone to migrate ($E_A(I) < E_A(Br) < E_A(Cl)$), followed by the organic A cations (with MA, ions generally are more mobile than in perovskites incorporating FA), and lastly, the B cation with significantly higher activation energies [12]. Additionally, a correlation between low activation energy and higher diffusion coefficients has been established, indicating that in the case of $MAPbI_3$, iodine ions diffuse the fastest [15]. Hence, for this work with the specified perovskite composition, the vacancy-mediated migration of I^- or Br^- is likely the predominant migration mechanism with FA^+ or Cs^+ in second place.

On a larger scale, the role of grains and their boundaries, as well as the broader implications of ion movement within the bulk and at interfaces, must be considered. While ion migration within the bulk certainly occurs, studies have shown that grain boundaries serve as the primary channels for ionic currents [18], although some ambiguity remains. Grain boundaries represent chaotic regions within a polycrystalline structure where edges of individual crystals intersect. In this open crystal structure, a multitude of uncoordinated components and defects converge, resulting in reduced ion activation energies and facilitating pathways for easy migration.

Consequences of ion migration are too numerous to be comprehensively discussed here. Thus, only selected effects of ionic movement are given. Distinguishing between bulk and interface effects is too simplistic, yet it is handy for a brief discussion. Within the bulk, ion migration has been mapped in situ using the previously mentioned photoluminescence technique, PLuB. Migrating ions impact the overall photoluminescence (PL) signal, typically leading to PL quenching, as demonstrated by e.g. Zhang et al. [19]. However, this work presents bright features or fronts of increased PL signal moving from the high-force anode to the low-force cathode, challenging the prevailing understanding of quenched PL due to non-radiative trap activation following halide migration. Reports of increased PL signal are uncommon but Luo et al. reported both increaes and decreases following PLuB in $MAPbBr_3$ single crystals [20] and a master thesis by Ravazzolo is a previous study with related research questions and a similar set up to this bachelor thesis also reporting bright fronts [21]. Further, it has been shown by Hoke et al. that under light exposure, halides migrate to form separate phases [22], a phenomenon that has since been documented by others [9]. Both the ion migration and phase segregation, caused by and increased with external stresses like heat, light, voltage, moisture and oxygen, can cause long term irreversible degradation, severely reducing perovskite device performance [9].

The movement of ions across the bulk inevitably results in some accumulation at interfaces, the transitional region between materials, where a complex and still poorly understood set of conditions exists. This leads to the next sections where junctions between different materials and the according processes are briefly described.

2.1.3 Junctions: The Interaction between Materials

Effects at the interfaces between functional layers or materials, while impossible to clearly separate from processes in the bulk, are actually more important to overall behaviour and performance of a given Pervoskite device. The accumulation of charges - both electronic and ionic - at the interfaces, and the subsequent alignment of energy levels and interaction of built-in potentials, screening electrical fields, and applied bias voltages, collectively dictate the characteristics of the perovskite device [12]. A critical distinction lies in the architectural design of these devices, categorised as either asymmetrical or symmetrical, the latter being employed in this study. Asymmetrical devices are the most prevalent, as they offer directionality for charges, facilitating the generation and extraction of current. Achieving this involves incorporating different materials and layers to inherently bias energy alignment and create selective barriers, thereby separating positive and negative charge carriers and driving them toward opposing electrodes. Conversely, symmetrical devices lack built-in directionality, rendering them not suited for practical photovoltaic applications. However, this architecture is advantageous for studying ion migration without directional preconditions and offers a clearer approach. Additionally, symmetrical architectures enable simpler fabrication processes, requiring fewer steps.
Given the symmetric devices employed in this study, no further discussion on asymmetric devices will be provided here (instead, see [12] or [23]). As previously noted, perovskites exhibit characteristics of electronic-ionic semiconductors, introducing additional layers of complexity to the typical junctions between standard semiconductors and metals. Merely examining electron and hole behavior falls short, as their movement significantly influences ion migration and accumulation, and vice versa. Key concepts to grasp the intricacies of these processes include Fermi level alignment and band bending, carrier injection from the metal electrode, formation of doped or depleted regions, accumulation of ions at interfaces with partial screening of present fields, and even more intricate and poorly understood mechanisms like electrochemical reactions and species migrations across junctions. [12]

From a simplified and idealised perspective, a semiconductor, in the absence of doping, possesses three characteristic energies: the valence band energy E_{VB}, representing the highest energy of occupied valence electron states, the conduction band energy E_{CB}, denoting the lowest energy of unoccupied or free valence electron states, and the FERMI level E_{F}, which, for an undoped semiconductor that is, lies in the middle of the other two energies. The Fermi level can be understood as a theoretical state with a 50 % quantum mechanical probability of occupancy, providing insight into the transition between occupied and unoccupied states. On a side note, the difference between E_{CB} and E_{VB} is called the band gap and photons of an equal or higher energy can be absorbed by semiconductors by exciting electronic carriers across the band gap, creating "free" charge carriers for photovoltaics. In the case of metals, only one energy level is of primary interest: the work function. This energy is analogous to the valence band energy in semiconductors, as it signifies the highest energy level of (densely!) populated states. However, because of the high amount of free states closely located to that energy level, carriers can easily move through the metal, distinguishing it from the valence band energy level. Above that energy level, no states are occupied, leading to its effective alignment with the Fermi level. Upon contact between a semiconductor and a metal, the semiconductor energies near the junction shift to align with those of the metal (the metals FERMI level has way higher population, dominating the semiconductors charge distribution), creating a built-in potential that drives local charge carriers. [7]
For perovskites, in addition to electron-hole pairs (and potentially dopants), ion migration and accumulation contribute to this redistribution, influencing the present field and partially screening it. Thus, a higher electrical field gradient is created near interfaces, with a lower gradient throughout the bulk. Under specific conditions, particularly high field gradients, electrochemical reactions may commence, leading to irreversible reactions, often involving reactive halides [9]. This may create energy barriers for charge carriers at the interface, degrading device performance. Furthermore, reports indicate that metal (Au) impurities diffuse into the perovskite layer, resulting in significant degradation [24][25].

In conclusion, a comprehensive theoretical explanation of the observed phenomena and intricate processes cannot be provided here. The scope of this work does not encompass a detailed presentation of the current understanding of perovskite's electronic-ionic dynamics. Moreover, gaps persist in our understanding, rendering a comprehensive theoretical framework currently unattainable, prompting further research.

2.2 Devices

In this work, a simple device architecture is employed, consisting of three functional layers and four component materials. The device configuration resembles half the stack of a pin-type PSC, as the layer between the metal electrode and the perovskite is electron selective, but it is characterised by symmetrical metal electrodes arranged laterally. The theoretical background of the architecture and materials will be briefly outlined to provide readers with the necessary understanding of the processes discussed later.

Architecture

The devices under study comprise a quartz substrate, a perovskite layer, an Electron Transport Layer (ETL), and metal electrodes. Both the spin-coated perovskite and the evaporated ETL cover the entire 15x15 mm sample. The ETL comprises two distinct sections: a 20 nm thick C_{60} layer directly on the perovskite, followed by a 7 nm thick bathocuproine (BCP) layer. These layers are evaporated successively. The electrodes are deposited using a specialised mask to create PLuB-compatible devices. Each sample has two channels each featuring a 10 mm long and $\approx$ 125 µm wide channel between two electrodes measuring $\approx$ 450 µm in width and 100 nm in height or thickness. Before converging to form the channel, the electrodes branch off to larger metal patches that are easily accessible with probes from a source measure unit (SMU), providing voltage. The inclusion of two channels enables two sets of measurements per sample, facilitating the application of only one polarity of voltage to each channel.

Materials

The quartz substrate serves solely as a foundation for the other layers, as there is no requirement for a conducting layer typically found on glass substrates for PSCs (e.g., an Indium Tin Oxide -ITO- transparent electrode). The perovskite material used in this work is a double cation double halide composition,$Cs_{0.18}FA_{0.82}$ Pb $I_{2.82}Br_{0.18}$, a typical mixture of different A and X components to improve characteristics, especially the bandgap and stability under various stresses such as heat and light. The addition of cesium enhances thermal stability [26], especially when formamidinium is also or solely included, as it provides greater stability compared to methylammonium-based PSCs [13]. Although methylammonium-based PSCs generally exhibit higher efficiencies, the use of triple (or even quadruple - minimal amount of Rb) cation varieties, particularly in perovskite-silicon-tandem cells, shows promise for achieving both high efficiency and stability [27]. Lead-based perovskites are predominant in research, despite efforts to

partially or fully replace the toxic heavy metal lead [28]. This research project exclusively employs lead-based perovskite due to the challenges associated with tin-based perovskites and their delicate fabrication processes [28]. Iodine and bromine are commonly used halides for the X component of perovskites. The specific ratio of iodine and bromine influences the characteristics of perovskites, such as bandgap and phase segregation [9]. Because the bandgap is mainly determined by the X^- and B^{2+} orbitals, varying the halogen composition facilitates easy bandgap tuning to optimize absorption. Therefore, the more electro-negative bromine forms perovskites with a deeper valence band and higher bandgap energy than $MAPbI_3$ [13]. The composition utilised in this work has a bandgap of around 1.6 eV based on the PL peak of $\approx 775\,\text{nm}$ ($E = \frac{h \cdot c}{\lambda}$), aligning with reported bandgaps for similar compositions [13]. This composition satisfies fundamental requirements, such as ease of synthesis and fabrication, overall stability, and compatibility with measurement conditions. Moreover, its relatively simple composition simplifies later analysis, allowing for clear attribution to the majority compounds. The ETL employed here consists of a layer of the so called buckminsterfullerene C_{60}, a ball-shaped molecule of 60 carbon atoms, and bathocuproine ($C_{26}H_{20}N_2$ / BCP), an organic and bulky ligand. C_{60} is an established ETL material, going back nearly a decade [29], with high electron mobility and adequate band alignment but often causing poor stability [30]. Although there are PSCs utilizing only C_{60} as ETL in the last five years [31], complementing it with a second thinner interlayer - e.g. BCP - has shown improvements of key PV characteristics (power conversion efficiency, general performance and long lasting stability) [30][32]. Together, this bilayer approach facilitates easier charge extraction with better energy alignment at the interfaces, enable trap passivation and improve stability[30]. Therefore, the utilisation of C_{60} / BCP provides valuable enhancements and more closely resembles a real PSC situation.

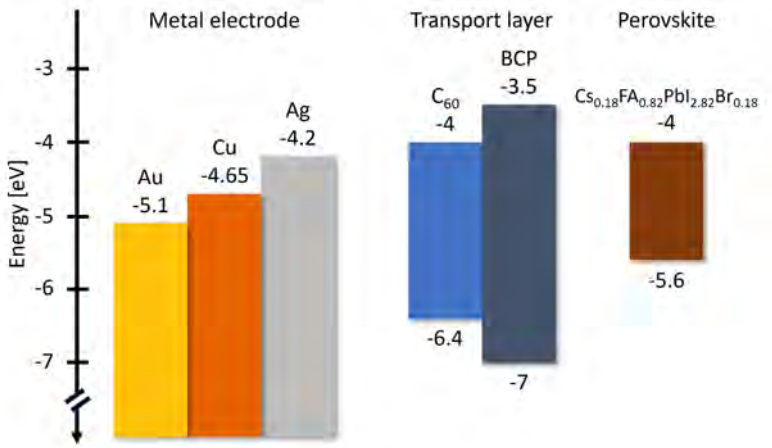

Fig. 2.2: Energy levels of all materials utilised in this study. Metal work functions from [23], transport layer from [33], and perovskite estimated from [34] and [35].

With a significant goal of this project being the study of different metals and their impact on ion migration, the choice of metals is key. Here, gold, silver and copper are used as they are most prominently used in perovskite research [23]. Especially gold and silver have been utilised numerous times and are therefore well studied. However, dedicated studies of their impact and especially concerning PL have been inadequately covered. All three metals have excellent conductive properties and can be easily implemented by simple thermal evaporation. Being most abundant and therefore the cheapest out of the three, copper qualifies as the best contender for commercialisation and widespread implementation. However, it is known to oxidise easily, whereas gold's chemical inertness renders it more favourable in that regard. Silver represents a compromise between the two being significantly cheaper than gold and more inert than copper. Other metals that would be interesting to study include aluminum and chromium as they see some adoption in research [23]. Moreover, they would provide further insight into the role of the work function as theirs is closely aligning with gold and copper respectively 2.2 [23].

2.3 Methods

In this section, the measurement methods are presented and their working principles explained. Besides the standard current-voltage curves, photoluminescence under bias is explored in detail. Afterwards, complementary methods such as X-ray diffraction, absorption and bias assisted charge extraction are shortly discussed.

2.3.1 Current-Voltage Measurements

The current-voltage (I-V) measurements are applied to a variety of electrical devices, providing key insights into basic electrical behaviour. While applying a voltage-sweeping bias, the current response of the device is probed and a characteristic shape is recorded. The current shape provides insights into fundamental mechanisms within the probed device and is used as standard characterisation of many devices. A basic resistor has a linear relation between increasing voltage and current. Diodes, have their own characteristic shape where only one polarity of voltage produces current, increasing exponentially after a certain threshold voltage is reached, whereas the other direction is blocked (up until the break through voltage).
For metal halide perovskite devices, I-V curves are also commonly provided, because of the various insights they provide. For solar cell devices in particular, I-V and especially current density-voltage (J-V) measurements are of great importance. Both light and dark conditions are used for measurements, as dark J-V curves give insight to the diode quality and with that recombination processes, whereas J-V under specific lighting conditions provides the power conversion efficiency, the most fundamental figure of merit for any solar cell. [7]
A common feature of I-V curves of perovskite devices is a current hysterisis where the current depends on the measurement history and different currents are measured for the same voltage. Tress et al. stated that:

> A rather broad consensus has been reached that hysterisis is a result of mobile atoms (and their vacancies). [16]

The causes of hysterisis are related to interactions of electronic and ionic carriers at the interfaces, depending on many factors, among others the lighting condition, ion density and mobility, I-V measurement voltage sweep speed [$\mathrm{V\,s^{-1}}$], the specific perovskite and architecture, etc. [16]
The exact reasons and consequences of current hysterisis are not relevant for this study, rather systematic differences between I-V curves of different metals would be. They would imply the metal has a significant effect on this phenomena, which is not expected. Instead, the metals displaying almost equal I-V characteristics both under dark and light conditions would speak for a benign effect.
Other than the metals impact, the impact of prolonged photoluminescence under bias measurements could be another relevant aspect for I-V measurements to provide. However, I-V curves are still a supplementary measurement technique to the central photoluminescence method.

2.3.2 Photoluminescence under Bias: Visualising Ion Migration

In order to image ion migration in metal halide perovskites, a sophisticated technique is required. With photoluminescence under bias (PLuB), a technique facilitating in situ observation of the effects of migrating ions, an indirect method is available. What this method is able to provide will be presented in the following.
Using an above-bandgap energy laser (here 405 nm), electronic carriers are excited within the perovskite, forming bound electron-pairs pairs called excitons. Then, these excitons can either be separated and extracted or they can recombine. Photoluminescence makes use of the radiative recombination of the excitons by detecting the emitted photons (here 780 nm) with spatial resolution of the device and spectral resolution of the emitted light. This general principle can be used to study different processes, which can be roughly grouped into two time regimes. Electronic processes occurring at short time scales in the femto- to milliseconds, represent one of the time scales. Here, electronic properties are of interest such as carrier lifetimes and recombination rates. On longer timescales, ionic motion in the sub-seconds to minutes regime, PL can also be employed to study the significantly slower processes of mobile ionic carriers. In order to do so, a bias voltage is applied, forcing mobile ionic carriers to drift through the perovskite. When the bias is applied, clear changes in the PL signal are observed (see fig. 2.4), which is attributed to ion migration. This provides secondary insight into the mixed optic-electronic-ionic processes at hand. Alongside the map depicting in-situ effects of ion dynamics, the current is measured while the bias is applied providing further insight into the different processes. The setup used for this study is closely resembled by the following figure 2.3 where the key components of a PL setup are shown.

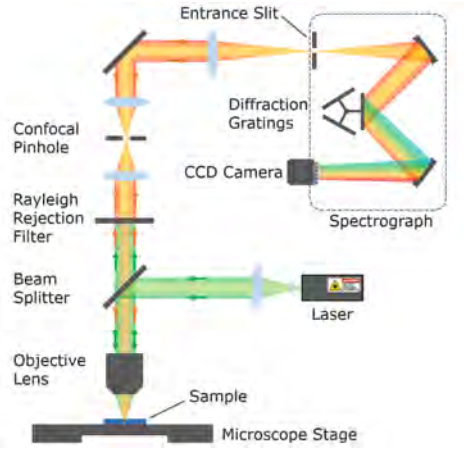

Fig. 2.3: A photoluminescence set up to conduct confocal RAMAN microscopy. [36]

Figure 2.3 depicts a photoluminescence set up similar to the one employed during this research project. In our case, a laser (405 nm) goes through a beamsplitter and is focused on the sample, which itself is on a movable PIEZO stage, using an objective (20x). The reflected light is passed through the beamsplitter and a long pass filter (488 nm) eliminates the reflected laser light. Now, only light of higher wavelengths (stemming from PL of the perovskite) is passed into a spectrometer where gratings and a CCD camera enable the spectrally resolved PL signal recording.
The recorded spectra can be analysed for given areas of the device, such as a specific line, to discern whether spectral changes occurred like peak shifts or emergence of other emission features. Migrating ions however, affect mostly the overall signal or PL intensity and therefore, usually the spectrally resolved counts of each point are summed to get one intensity value for each pixel of a map. Together, they provide a simple way to visualise ion migration by emerging dark or bright features of a map that is projected from the measured device area. An example of that is depicted in figure 2.4 below.

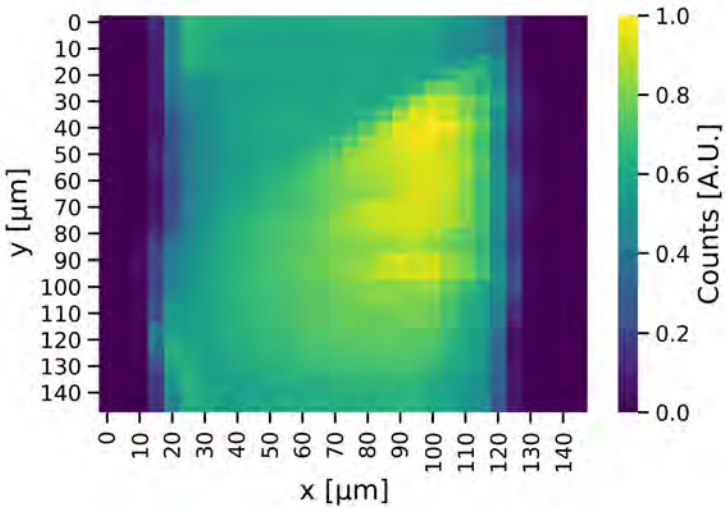

Fig. 2.4: A photoluminescence map of the perovskite in between two metal electrodes. The spectrum of each pixel is summed and plotted as normalised intensity.

In the context of this research project, a quantitative analysis of the PL signal is not possible, prompting the normalisation of each map individually. This results in PLuB maps that depict features in a comprehensive way which will be presented and discussed in later sections.

2.3.3 Complementary Measurements

Other methods used to characterise the devices probed entail an optical microscope, an X-ray diffraction crystallographer, a total absorption spectrometer and a profilometer setup. Each will be briefly introduced to justify the quick coverage of the results in later sections.
An optical microscope uses visible light and lenses to magnify the probe enabling detailed visualisation. Here, lenses with a resulting magnification of 10x, 50x and 100x, have been employed to study the perovskite film and the metal electrodes.
X-ray diffraction (XRD) crystallography provides insights into the crystal structure of the studied perovskite film. A crystal structure has periodic planes that diffract X-rays in a specific way enabling characterisation. A highly crystalline structure will result in an angle-resolved spectrum with well defined and sharp peaks. It is then possible to attribute the measured peaks to Miller indexes and confirm expected crystal structures. This method is used for metal halide perovskite devices to ensure proper crystallisation into a uniform phase [37].
A crucial measurement technique for solar cells is the absorption spectroscopy as the capture of light is one half of what is required for photovoltaics, with charge extraction being the other part. In order to probe the spectral absorption of a sample, light of a given spectrum is directed at the sample, however there are multiple ways to proceed. In a simple setup, the detector is placed behind the sample receiving transmitted light. This neglects the contribution of reflected light which is not regarded in the simple absorption spectroscopy. By introducing an integrating sphere, reflected light is captured too, facilitating total absorption spectroscopy. This then provides the spectrally resolved absorption of the device providing insight into its optical characteristics.
Finally, a profilometer was employed to study film thicknesses of the spin coated perovskite layers. In a profilometer, the displacement of the stylus while moving across the surface of the sample is measured. By scratching a device, a trench is created which the stylus is dragged across. The height over position is recorded and provides insight into the film thickness.

Applying the different characterisation techniques provides an overview of different aspects of the employed devices. With the theoretical background now covered, the following experimental section 3 provides a detailed list of all conducted fabrication and measurement steps.

3 Experimental Section

The experimental section will provide a detailed summary of the entire process from device synthesis to measurement protocols and analysis.

3.1 Device Synthesis

Chemicals

The precursor solution was mixed using PbI_2 (99.99 %) purchased from TCI Chemicals, FAI (99.99 %) purchased from Greatcells Solar and CsBr (99.9 %) was purchased from Sigma Aldrich. Hellmanex III, acetone, isopropanol, DMF ((99.8 %, anhydrous) and NMP (99.5 %, anhydrous) were purchased from Sigma Aldrich. The chemicals were used as received. For the evaporation, C_{60} (99.9 %) was bought from Sigma Aldrich, Bathocuproine (BCP, > 99.5 %) was bought from Ossila, copper (99.99 %) and silver (99.99 %) pellets were purchased from Kurt J. Lesker and gold (99.99 %) pieces were purchased from Drijfhout.

Synthesis of the Perovskite Solution

The research project encompassed fabrication of different device batches, however, only two (number 3 and 6) are of importance as solely devices of those batches were used for the data presented in this report. Thus, if different, the three numbers (the first indicating the recipe reference value, second number for batch 3, and third for batch 6) for each value in the following section will be presented to indicate potential batch differences.

The synthesis of the double cation double halide lead based perovskite included the following steps. Firstly, the three salts PbI_2 (614 mg_r, 673.3 mg_3, 761 mg_6), FAI (189 mg_r, 207.2 mg_3, 234.4 mg_6), and CsBr (51.5 mg_r, 57.5 mg_3, 63.8 mg_6) were weighed into a vial and dissolved using DMF and NMP (9 : 1, 1.4 mL_r, 1.54 mL_3, 1.734 mL_6) resulting in a bright yellow and clear solution of $\approx 0.9\,mol\,L^{-1}$. The higher weights come from correcting weighing errors. Batch 6 deviated less than 0.1 % from the recipe. Same for batch 3, except for CsBr, which is 1.7 % more than intended. The solution was then stirred at room temperature ($\approx 24\,°C$) over night. Before spin coating the solution, it was heated to 100 °C for 15 min and shortly left to cool down to room temperature again. Now the solution was filtered using a PTFE filter (0.22 µm) and the resulting solution was used for the spin coating process.

Automated Spin Coating

The key fabrication step of spin coating the perovskite precursor solution was conducted not manually, but using a robot: The SpinBot by Sciprios [38].
Before spin coating, the 15x15 mm quartz samples were cleaned using a brush, water, and Hellmanex III, then sonicated for ≈ 15 min first in deionised water, then IPA, and finally in acetone. To finish the cleaning process, the samples were cleaned for one minute in a 100 W plasma using a Diener Zepto low-pressure plasma cleaner. For the actual spin coating process, the ≈ 70 µL of precursor was statically dispensed shortly after which, the first step of 2000 rpm for 10 s with an acceleration of 200 rpm s^{-1} was conducted. A second step of 5000 rpm for 30 s with an acceleration of 5000 rpm s^{-1} followed suit. Here, gas quenching was employed with dry N_2 being dispensed by a nitrogen gun under 5 bar of pressure with $5 - 10$ cm of distance for the duration between 25 s and 10 s before the end of the total spin coating process. Finally, the samples were annealed at 100 °C for 10 min resulting in visually uniform and dark films.

Thermal Evaporation

Both the two layers of the ETL and the metal electrodes were deposited using thermal evaporation in vacuum (10^{-6}-10^{-7} torr) conditions. An Angstrom Engineering evaporator was used to evaporate 20 nm of C60 onto the perovskite film and subsequently, 7 nm of BCP was deposited. For this step, no mask was used, thus the entire sample is covered with the bilayer ETL. For the metals, a mask was used which will be described in further detail in the next paragraph. A lower rate of 0.1 Å s^{-1} for the first 10 nm and a higher rate of 1 Å s^{-1} for the latter 90 nm, which was the same for all metals.

3.2 Production of the Evaporation Mask

The device architecture was specifically designed to allow for an efficient production of devices to study the different metals. Thus, a new evaporation mask was required which was created in collaboration with the support staff and mechanical workshop at AMOLF. For this purpose, a stainless steel (304) sheet (150 µm thickness) was cut into a mask design by wire electrical discharge machining (WEDM) using a Fanuc Robocut α-c400ic. The mask and a brass wire (250 µm diameter) are submerged in de-ionised water and a high voltage is applied between them to precisely erode away the metal through repeated electrical discharges (sparks) [39]. In order to achieve the fine details of the mask - in the few hundreds of micrometers - the WEDM was employed in second skimming mode, because the usual rough cut mode would not allow for the required

precision. However, due to the short time of the project, the process could not be optimised fully which resulted in not perfectly uniform electrodes (like those utilising UV-lithography masks).

3.3 Measurement Methods and Protocols

Current-Voltage Measurements

For the current-voltage (I-V) measurements a Agilent B2902 A source measure unit was employed. The standard I-V parameters used during experimentation are a -1 to 1 V sweep with a sweep speed of $\approx 250\,\mathrm{mV\,s^{-1}}$.

Photoluminescence under Bias

Photoluminescence under bias measurements were conducted using a WITec alpha300 RS confocal microscope with a 20x magnification air objective microscope (Zeiss EC Epiplan 9903). The laser used is a 405 nm wavelength continuous-wave laser (Thorlabs S1FC405). Using reflection mode, and with a 488 nm long pass filter, the luminsecence was collected by a WITec UHTS spectrometer with a $600\,\mathrm{g\,mm^{-1}}$ grating. The laser power was 30 µW for all scans and the integration time for each spectrum was a constant 150 ms. The maps take 3 min40 s and are 150x150 µm with 30x30 pixels, with a laser spot size smaller than the pixel size.
For applying bias, the same Agilent B2902 A source measure unit was utilised. A ± 5 V or ± 10 V bias was applied for 120 s with 0 V before and after the bias.

X-ray diffraction crystallography

The X-ray diffraction crystallographer employed here was a Brucker D8 diffractometer in Bragg-Brentano configuration. Co-Kα ($\lambda = 1.79$ Å) radiation was used with a measuring range from 12 to 35° in 0.02° steps with an integration time of 0.1 s.

UV-vis absorption spectroscopy

For the UV-vis absorption spectroscopy, a Lamda 1050 spectrophotometer by PerkinElmer was employed using an integrating sphere. The spectrum was acquired from 300 to 900 nm.

4 Results

In the main section of this study the various results are categorised and presented. This section aims to lay out the results gathered in a comprehensive way in order to build a basis for further discussion and research. The results are clear to the extend that consistent trends and features can be differentiated and individually presented. However, they illustrate the complexities of optic-electronic-ionic interplay in metal halide perovskites as interpreting and explaining the gathered data provides challenges. Therefore, results and discussion are separated into two sections in order to clearly distinguish between what are observations and what are explanations. However, this only applies to the photoluminescence measurements. For the following characterisation the results of the different methods will be presented and shortly discussed.

4.1 Characterisation

At the outset of this research project, different solvents and spin coating parameters were examined to determine the optimal fabrication method for producing high-quality perovskite films. Subsequently, the devices underwent characterisation using X-ray diffraction (XRD), UV-vis absorption spectroscopy, and profilometry. Additionally, images to study the morphology were taken using an optical microscope.
X-ray diffraction crystallography confirmed the uniform crystallisation of the perovskite film. One XRD scan is presented in 4.1, illustrating intensity over the angle of reflection with additional Miller indexing of perovskite crystal peaks.

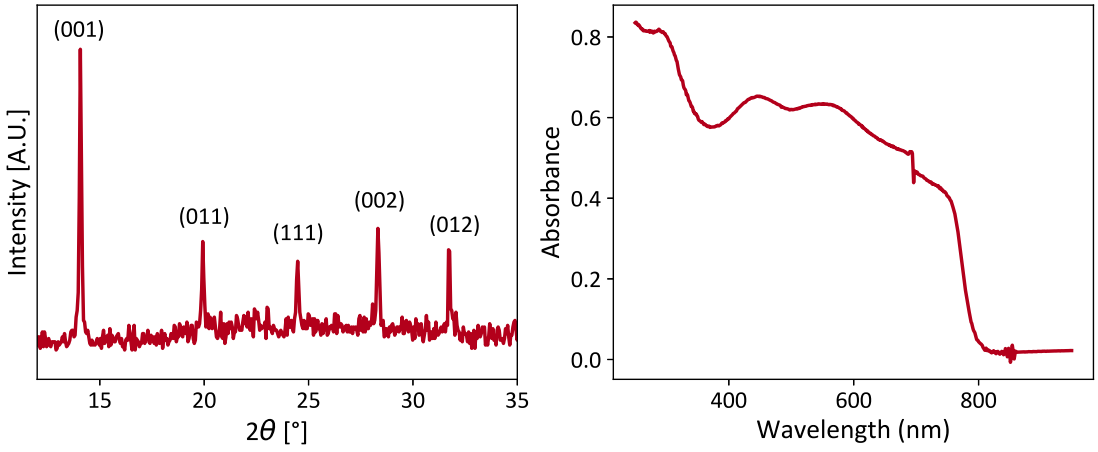

Fig. 4.1: An X-ray diffraction scan with Miller indexes and an UV-vis absorbance spectrum to illustrate optical properties of the perovskite.

UV-vis absorption spectroscopy was also employed to further investigate the optical properties of the devices. In the absorbance spectrum 4.1, two small features at approximately 700 nm and 850 nm are identified as measurement artifacts caused by grating switching. Disregarding these artifacts, the spectrum reveals a clear onset of absorption beginning just below 800 nm, indicative of the bandgap with an energy of approximately $\approx 1.6\,\text{eV}$. Additionally, the absorbance spectrum demonstrates that the devices are effective photoabsorbers, although their efficiency could be improved. The devices are not fully black under room light conditions but instead exhibit a slightly transparent dark brown hue, indicating the potential for enhanced absorbance through improvements in composition quality, fabrication techniques, and layer thickness.
In conjunction with XRD and UV-vis absorbance measurements, optical microscope images underscored the uniform crystal structure. However, some images, particularly toward the center of the sample, exhibited black spots or pin holes within the film and even cracks in the crystal 4.2.

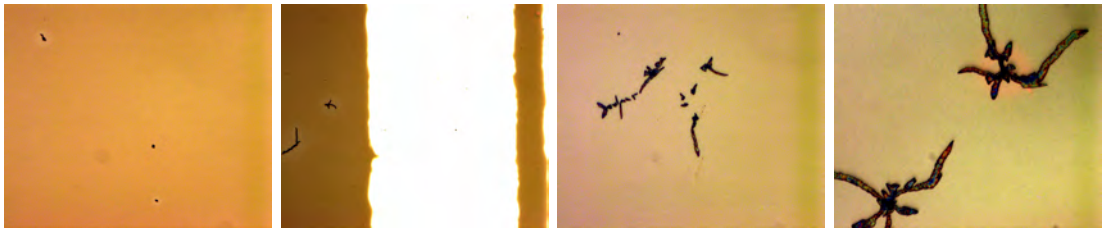

Fig. 4.2: Four optical microscope images of the perovskite film where 2-4 are three weeks older than 1. 1: (10x), 2: (10x), 3: (50x), 4: (100x).

While the resolution of the optical microscope was insufficient to resolve small crystal grains, the black spots were discernible. Exposure to various stresses such as light, voltage, PL measurements, oxygen, and moisture led to the formation of cracks throughout the crystal, emanating from these black spots. This behavior may be attributed to the severe degradation of the perovskite film along grain boundaries, exacerbated by its direct contact with the atmosphere (only 27 nm of ETL in between). However, in this case, these effects are not expected to significantly impact the measurements conducted in this research project, as long-term stability and high performance are not primary concerns. Nonetheless, this factor should be considered when analysing older samples exhibiting different behaviors.
In conclusion, the characterisation results indicate the production of high-quality perovskite films suitable for the objectives of this research project. Subsequent sections will delve into the presentation of data relevant to the research question.

4.2 I-V Curves

The cornerstone measurement for any electrical device, the current-voltage scan, has been thoroughly conducted throughout in this work. Each device underwent measurements under both ambient room light and dark conditions within a range of -1 to $1\,\mathrm{V}$ before, in between, and after PL measurement sessions. This extensive dataset facilitates the examination of broad trends, such as the effects of PL measurements and the influence of metals on the currents.
Firstly, the general shape of the I-V curves, which remains mostly consistent under all conditions, is outlined. A linear increase in current with increasing voltage suggests simple resistive behavior, while a sudden, more rapid increase in current after reaching a threshold voltage indicates diode-like behavior. Furthermore, variations in currents depending on measurement history or scan direction, known as hysteresis, particularly in perovskite devices, imply ion migration and accumulation [12]. These three features are partially present in the devices studied in this work, as depicted in figure 4.3.

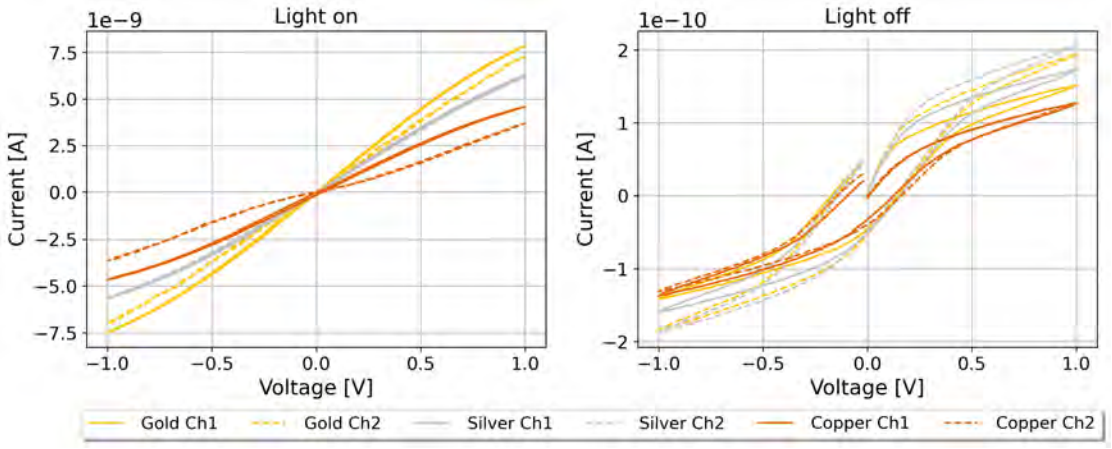

Fig. 4.3: *I-V* scans of different metals in ambient room light (left) and dark condition (right). Each sample consists of two channels with the same metal.

Under ambient light conditions, the shape of the I-V curves resembles that of a typical resistive electrical device, with mostly linear increases and minimal hysteresis. This trend is observed across all metals, although copper exhibits some non-linearity. Notably, for channel two of the copper device, the slope is steeper for voltages above $0.25\,\mathrm{V}$, and a slight hysteresis is visible, particularly in the negative voltage regime. This hysteresis is attributed to ion movement impacting the negative voltage regime due to the

voltage's progression from 0 to 1 V and then into the negative range, where current is then impacted by previously migrated ions. However, the observed impact is minimal, suggesting that the current is dominated by electronic behavior. Regarding the varying current magnitudes observed for different metals, a definitive trend of specific order ($C_{\text{max, Au}} > C_{\text{max, Ag}} > C_{\text{max, Cu}}$) could not be confirmed upon comparing I-V scans.
Under dark conditions, the results exhibit significant changes, with current magnitude decreasing by over one order of magnitude, and hysteresis dominating the overall shape of the curves. In the absence of photo-generated electrical carriers, the overall current decreases, allowing the ionic contribution to become more pronounced, resulting in a more prominent hysteric current trace. The observed hysteresis loop resembles typical behavior seen in other hysteric electrical devices [40] and even in other fields such as magnetism [41]. The I-V scans under dark conditions provide valuable insights, indicating that metals do not significantly influence the hysteresis response in the devices, at least within this current range. However, there appears to be a trend suggesting that copper leads to overall lower currents across different conditions and fabrication batches, although this difference is not significant enough to make broader conclusions.

4.3 Photoluminescence under Bias

Studying ion migration via Photoluminescence under Bias (PLuB) resulted in a multitude of observed behaviours which do not have established models and mechanisms with which to confidently explain the results. Thus, in the following, the different trends are presented alongside qualitatively descriptions. First, general trends are presented, like the known light soaking effect or the observed bright fronts. Later, metal specific results are presented concluding the PLuB results section.

4.3.1 Light Soaking

Perovskite devices often show the effect that constant (not too high intensity - otherwise the perovskite will be damaged) illumination results in an increased performance and when probing with PL, an increase in signal due to passivation of trap states and thus, more radiative recombination [42]. However, light soaking is dependent on the specific perovskite and its fabrication as it may also cause degradation and PL quenching [19].
For the devices probed in this project a significant increase in PL signal was observed in every fabrication batch, of which, two examples are shown below in figure 4.4. However, not only was the overall PL signal increasing but the peak position of the emitted light shifted towards higher wavelengths which is depicted in the same figure 4.4.

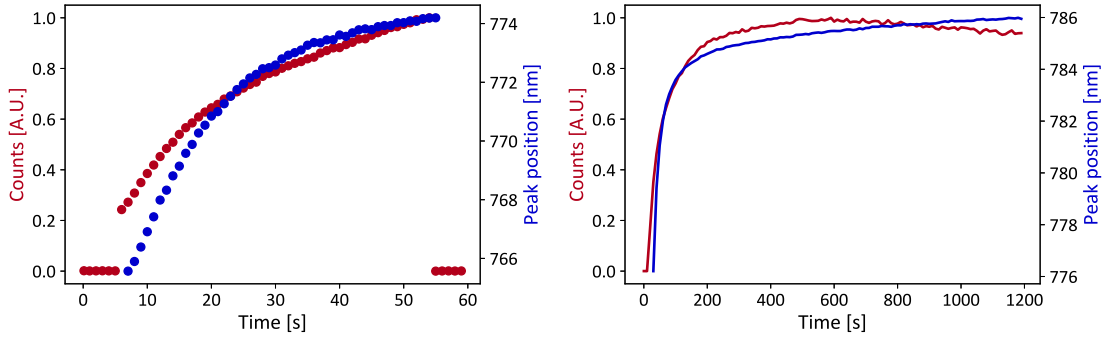

Fig. 4.4: Time evolution of total photoluminescence counts and spectral peak position. The figure on the left depicts a one minute time frame and the right hand figure tracks their development over 20 minutes in a differently fabricated perovskite.

Figure 4.4 clearly demonstrates the light soaking effect on a shorter and long timescale. The overall PL counts increase for the first few minutes but begin a decreasing trajectory afterwards. The initial positive effect of illumination is then suppressed by more destructive mechanisms. Both are probably related to ion migration as the local increase in energy and excitons leads to electro-ionic interactions leading to changes affecting the recombination processes.

The shift in PL peak position is most likely also related to these dynamics processes as energy levels for recombination are intricately dependent on the local crystal structure. The initial difference of PL wavelength proposes differences in the perovskite which can be attributed to overall batch to batch differences but it should be mentioned that the 20 minute measurement was conducted using a perovskite dissolved in DMF:DMSO instead of DMF:NMP which was used for all batches since this early one. Thus, a quantitative comparison between the two is not applicable, but the qualitative similarity of observed peak position red shift holds. Interestingly, the peak position still increases in wavelength even after 20 minutes, although the shift is only in the order of single nanometres.

Light soaking is a prominent feature in this work as it will come up again influencing the PL scan discussed later. Even though it is related to ion migration it is not the specific kind of interest to the research question tackled here.

4.3.2 Bright Fronts

One of the most striking features observed in the study is the presence of bright fronts traversing the channel during applied biases from the anode towards the cathode. This phenomenon was consistently observed across all metals, albeit with notable differences in appearance. The intensity, extent, decay, and velocity of these bright fronts systematically varied depending on the specific metal used and the magnitude of the applied voltage. The emergence of these bright fronts raises intriguing questions as they have not been extensively reported in literature, where dark fronts or photoluminescence quenching due to ion migration are more commonly discussed phenomena [11]. However, the detailed analysis of the observed data provides valuable insights into the underlying processes.

To clarify, in a PL map, the dark sections on the left and right-hand sides correspond to the metal electrodes, which block the laser, resulting in no detected PL signal. The baseline signal is removed and the overall counts are normalised for simplified presentation, given the challenges associated with quantitative analysis under varying experimental conditions. For the following depictions of PLuB, a scan takes 220 s of which the first 30 s are not biased; then the bias (of ±5 V or ±10 V) is applied for 120 s; with the rest of the scan being unbiased again. This facilitates the differentiation of the immediate effect of bias and the start of the decay process.

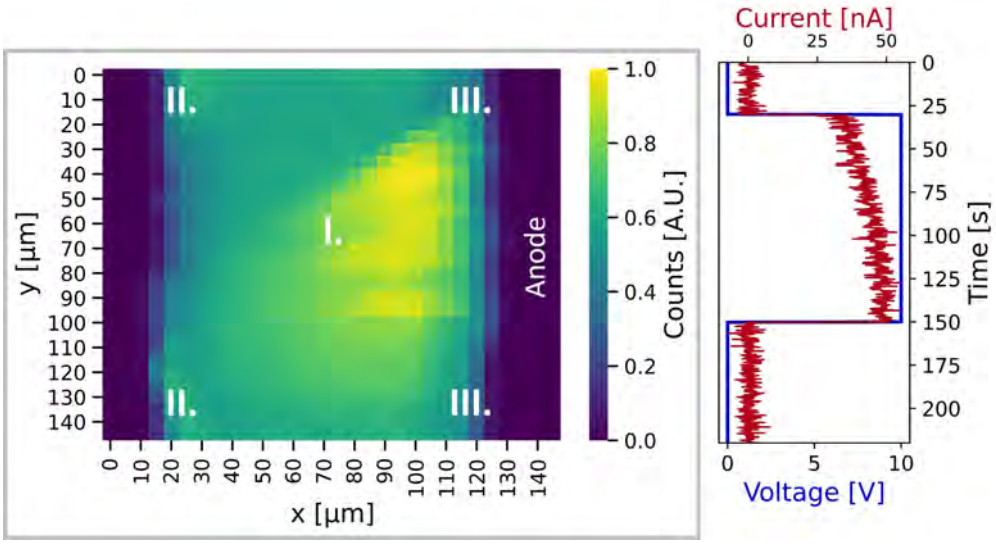

Fig. 4.5: A photoluminescence under bias map with summed and normalised intensity. Applied voltage and resulting current over time are presented on the right.

Figure 4.5 exemplifies a particularly intense bright front (**I.**), characteristic of silver, spanning most of the channel during a 10 V bias. The front exhibits a $\approx 40\,\%$ increase in PL intensity compared to the rest of the channel, demonstrating the profound impact of bias-induced ion migration on PL. In figure 4.5, the onset of the front is clearly visible, as well as the point where bias is no longer applied coinciding with a sudden decrease in the fronts brightness around the y value of 100 µm. To further enhance comprehension of the PL maps and their evolution in time, the current - recorded simultaneously - is depicted alongside with its time axis synchronised to that of the PL map.
During the unbiased section preceding the bias application, the channel appears mostly uniform in brightness, albeit with subtle features near the cathode and anode. On the left side, near the cathode (**II.**), a slightly brighter region of a few pixels is visible, most likely stemming from another feature discussed in the next section 4.3.3. Near the anode on the right (**III.**), the opposite presents itself, a slightly quenched PL signal which resembles the last general trend presented in section 4.3.4.
Of far higher intensity however, is the bright front (**I.**) appearing during applied bias, exhibiting three discernible regions: firstly, close to the anode the increase in signal is constrained by the present dark feature, secondly, the intensely bright center of the front, about $10 - 30$ µm into the channel, and finally, a shallower front extending towards the cathode. The velocity of the bright front is estimated to be approximately $1\,\mu m\,s^{-1}$, considering its traversal of 100 µm within less than two minutes. The main increase in signal does not go beyond the midpoint of the channel and abruptly decays upon deactivating the bias. Interestingly, the current shows a slight increase over the two-minute bias application, reaching a peak of 50 nA by the end, which is comparable to those of other scans as they share the order of magnitude. However, the magnitude and shape of the current evolution varied significantly between different metals, batches, samples, and applied voltages. While a more detailed analysis of the time-current data is deferred to a later section 4.4, the observed trends underscore the complex interplay between ion migration dynamics and device behavior, influenced by material properties, applied biases, and fabrication conditions.

4.3.3 Increased Signal at Cathode

Another consistent feature observed across all metals is an increase in photoluminescence (PL) signal at the cathode (**II.**), opposite to the bright fronts. However, this feature exhibits fundamentally different characteristics, distinguishing it as a separate process. Unlike the bright fronts, which appear during bias application, this feature is actually quenched by bias, disappearing for the duration of applied voltage. Remarkably, it initially arises from repeated application of voltages, gradually manifesting over the course of a measurement session. Furthermore, once established, this bright feature persists and even intensifies if the device remains unbiased and unmeasured over extended periods. An example of these behaviours is presented in the next figure 4.6.

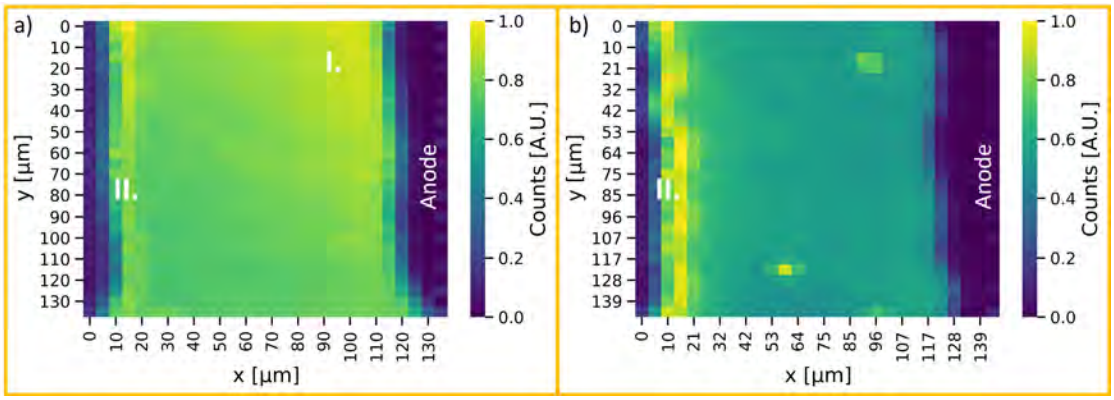

Fig. 4.6: Photoluminescence maps with summed and normalised intensity. Map a) was recorded after a 15 V bias was applied previously. Map b) depicts the same device in a different area after 1.5 h.

Figure 4.6 presents two PL maps depicting unbiased scans, confirming that the observed increase in signal (**II.**) is not caused by applied voltage. Notably, the enhanced signal at the cathode persists even after 1.5 hours of storage in a glovebox, indicating a longevity distinct from the migrating and accumulating ions observed in bright fronts. Moreover, there is no discernible diffusion of this feature, suggesting a mechanism different from ion accumulation, as it remains localised and does not disperse over time. Interestingly, applying bias temporarily quenches the signal, but it re-emerges afterward, often more pronounced than before, demonstrating the role of applied bias in causing this feature. While the influence of metals on this feature is evident, with gold exhibiting it most prominently, followed by copper, the underlying mechanism is likely intrinsic to the perovskite composition. For the silver devices, this feature was observed too, however, it

was more challenging to clearly distinguish it because of low intensity and mixing with a bright feature more correlated to a decaying front as depicted in figure 4.13. Further discussion on the mechanisms behind this feature and the metal's role will be presented in a later section.

4.3.4 Dark Front on Longer Timescale

In addition to the observed increases in PL signal, another noteworthy trend emerges — a gradual decrease in signal intensity at the anode over an extended period (**III.**). This feature shares similarities with both the reported bright fronts and the increase in signal at the cathode. Firstly, it originates from the anode, coinciding with the emergence of bright fronts, resulting in overlapping features that are challenging to distinguish. Secondly, this quenching does not manifest as a clear front but rather as a gradual darkening over time. Similar to the cathode signal increase, it appears incrementally with repeated biased scans, without any discernible decay within a single measurement session. The metals have influence on the appearance of this feature too, but it has been observed for all.

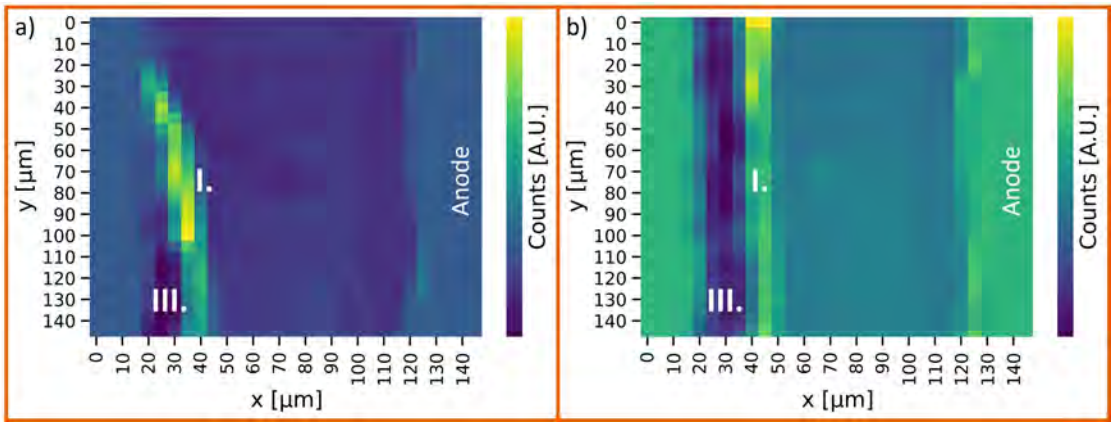

Fig. 4.7: Two photoluminescence difference maps where each pixels summed intensity is subtracted from an initial unbiased scan. a) −10 V bias is applied. b) Same device and area after multiple other scans (0 V).

Figure 4.7a) illustrates a typical copper 10 V scan using a different visualisation method, where a reference scan is subtracted from the total PL counts to highlight features induced by bias. Similar to a normal PL map, the bright pixels represent an increase in signal, thus showing a bright front (**I.**), which extends only for approximately 30 µm. This kind of small extend but strong increase in signal is regularly observed for copper.

Besides the bright front a second features is emerging from the same anode (**III.**). It is visible for y-values of over 100 µm where the bias is turned off. Here, a significant quenching of the PL counts is present pushing the bright feature to its side.
In figure 4.7b) the subsequent non biased scan is depicted showing the decay of the bright front (**I.**) next to the unchanging dark feature (**III.**). Subsequent unbiased scans reveal the persistence of this dark feature, which gradually extends across the channel with further biasing. However, never has this dark feature been observed to reach across the channel as it is spatially limited to a third of the channel. Applying an opposite bias slightly increases the brightness again but it does not revert the quenching completely. However, this has not been studied in sufficient detail, so it is unknown whether applying opposite bias multiple times or a long relaxation revert this dark feature.
Same as for the previous two features, this trend generally appears for all metals but with differences in specific characteristics. Copper is definitely the most prominent when it comes to this dark feature.

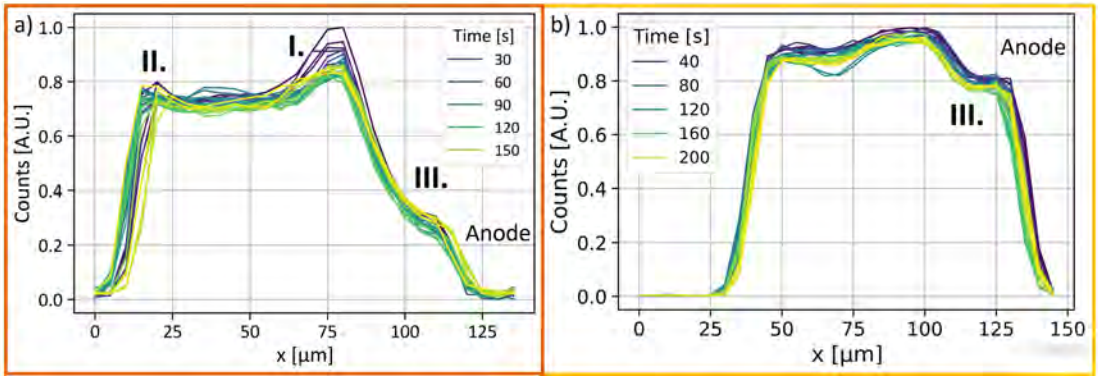

Fig. 4.8: Two photoluminescence line plots of normalised intensity (time ≡ y-axis of device channel) of unbiased (0 V) scans. a) Copper. b) Gold.

Figure 4.8 provides further insight into the characteristics of the dark feature (**III.**), comparing scans for copper (a) and gold (b). Both of them do not have any bias applied and no change in the feature within the roughly three minutes of scan duration is visible. The quenching is not uniform however, as there is a clear intensity gradient observable as the intensity grows reaching further into the channel. The dark feature for copper spans approximately 50 µm but is also affecting the decay of the bright front (**I.**) next to it in the channel. The feature (**III.**) itself seems to be split in two section where for the first 15 µm of the channel an increase to about 25 % of the normalised signal is reached and a second steeper section leading up towards the decaying peak signal at $x = 80$ µm.

For Gold the channel has less relative quenching as the dark plateau lies at 80 % of maximum PL signal. Moreover, the width of the dark feature is about half that of coppers. The steep rise in signal right at the anode is abruptly cut off and goes into the quenched plateau. Then the dark feature smoothly translates into the bright center of the channel around $x = 100\,\mu m$ where a previous dark front is slowly fading out. The dip around $x = 100\,\mu m$ and 100 s is a measurement artefact related to the laser and thus not of significance.

In summary, these observed features demonstrate a dependence on the metal electrode, emphasising the importance of characterising the metal-specific influence on ion migration, as further elucidated in the subsequent section.

4.3.5 Metal Specific Features

Given the primary focus of this project on characterising the metals' impact on ion dynamics in perovskite, a more detailed look at their effects on the presented general trends is due. Thus, an overview of how the appearance of the general trends is shaped by each metal is provided here.

Gold

Devices featuring gold electrodes are distinguished by longer-lasting but slower and less intense bright fronts. These fronts also necessitate higher voltages to appear compared to those for copper and silver. Additionally, in some cases, devices with gold electrodes did not produce detectable fronts at all. However, the bright feature at the cathode was most prominent for gold, exhibiting the highest relative intensity. Although the dark feature was observed for gold, it did not extend as far as it did for copper, and the quenching was less significant. The reasons for these differences will not be discussed here but merely presented to provide a proper basis for further discussion and research.

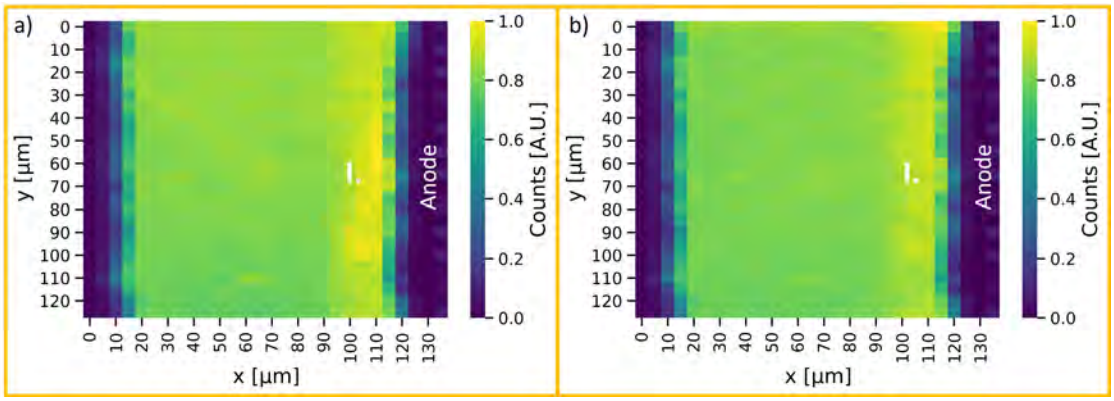

Fig. 4.9: Photoluminescence maps with summed and normalised intensity. Map a) 10 V bias scan. Map b) subsequent 0 V unbiased scan.

Figure 4.9 depicts a typical bright front and subsequent decay for gold (**I.**). The front (a) only extends into the channel for up to $y = 30\,\mu m$, and its relative intensity is so low that it is challenging to clearly distinguish it in the PL map. This kind of shallow front has been consistently observed for gold, significantly differing from the fronts observed for the other metals. The decay (b) is also typical for gold, characterised by long decay times and no movement of the remnants, as the signal slowly decreases in intensity. Another feature of gold's bright front is a higher threshold voltage required. For voltages of ±3 or ±5 V, barely any front is visible, and even for 10 V, a clear front is not consistently seen, with some devices not showing any front at all. An example of what a biased scan without a clear front would look like is shown in the next figure 4.10.

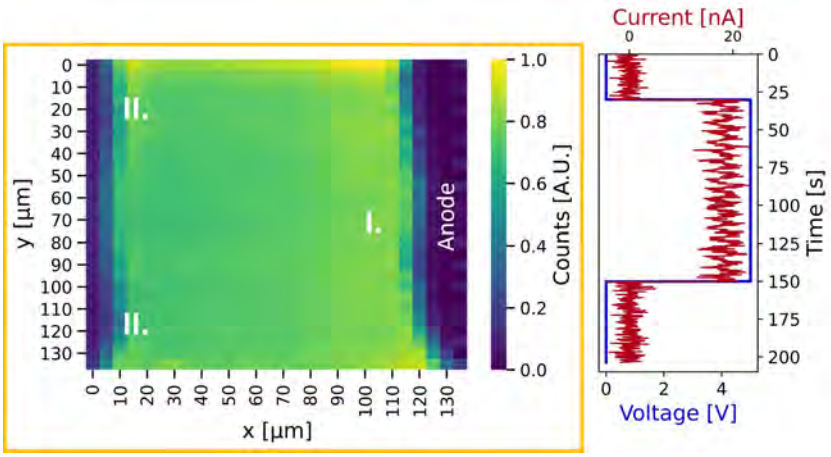

Fig. 4.10: A photoluminescence under bias map with summed and normalised intensity. Applied voltage and resulting current over time are presented on the right.

Figure 4.10 illustrates a biased scan without a clear front (**I.**), showcasing multiple features, including the slight increase in intensity due to the bias originating from the anode. The first line of the scan is brighter than the others, related to light soaking which is not relevant here. Additionally, the increased signal at the cathode (**II.**) is observed throughout the scan, and as usual, the light-up at the cathode is quenched during applied bias.
Concerning the bright front (**I.**), it is clear that a bias is applied across the channel as the current shows a normal shape and magnitude for 5 V. Still, no real front movement is visible indicating higher voltages required for the appearance of proper fronts.

As already stated in the section of the bright cathode feature (sec. 4.3.3), is most intense for gold, appearing more often and with a higher relative increase in signal. Figure 4.6 depicts two examples of this aspect (**II.**).
For the dark feature on longer timescales, gold is less prominent. Figure 4.8 shows one line plot of this feature (**III.**) where it was most intense for gold. Still, it is significantly less pronounced compared to the copper one depicted in the same figure. Other times this feature was observed, it had even less intense quenching. The extent of this feature would also vary; for example, another device of the batch showing the dark feature had only about half the extent. However, qualitatively, they showed similar characteristics as bright fronts would be affected by the appearance of the quenched area, starting and decaying next to it.
Overall, gold exhibits distinguishing characteristics in all discussed features, providing a basis for later discussion. An overview of quantisation of the features observed for gold will be presented alongside the other metals in table **??**.

Copper

Devices fabricated with copper electrodes exhibited the brightest fronts and most intense darkening at the anode. Additionally, a significant increase in signal at the cathode was observed for copper, although less intense than that observed for gold. A notable similarity between copper and gold is the extent of the fronts, staying close to the anode rather than traversing most of the channel as seen in silver devices. With the stronger signal in copper devices comes a faster decay, as the relative intensity mostly diminishes within the subsequent biased scan.

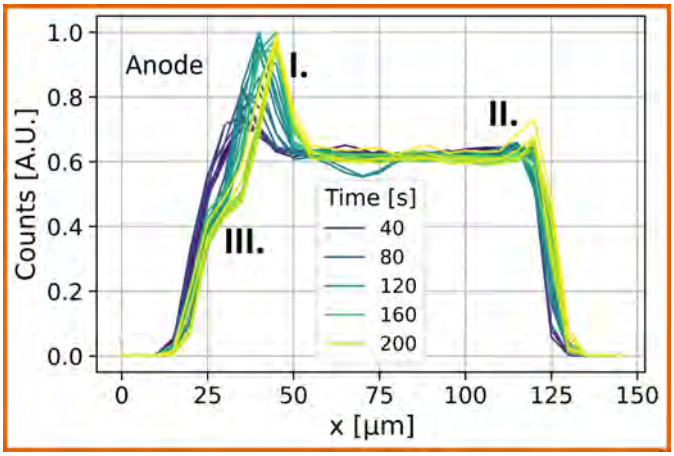

Fig. 4.11: A photoluminescence line plot of normalised intensity (time ≡ y-axis of device channel) of 10 V bias.

Figure 4.11 illustrates a combination of almost all features observed for copper. The high-intensity bright front (**I.**) builds upon an already increased signal at the anode from a previous biased scan. Thus, the first lines where no bias is applied yet already have an increased signal, with a hint of the appearing dark feature (**III.**) around 30 µm. With the bias being applied, there is a rapid increase in signal, and a front appears, extending over 35 µm into the channel. In quick succession, the prominent dark feature emerges from the same anode, cutting off the bright front and stabilizing by the end of the scan duration. The peak of the bright front shifts slightly after the bias is turned off around 150 s into the scan, settling at 100 µm. The cathode lighting up (**II.**) occurs for the last lines, indicating further increase in signal after the scan.
This depiction clearly highlights what distinguishes copper from the other two metals: sharp and intense bright fronts, strong quenching at the anode, and a significant increase in signal at the cathode. The bright fronts are more intense than those observed in gold but with less extent than those seen in silver devices. Previously shown plots, such as Figures 4.7 and 4.8, further underscore the general characteristics of copper.

Silver

Characterizing the effect of silver electrodes poses challenges due to substantial variations in results. Overall, silver electrodes exhibited the fastest and farthest-reaching bright fronts with high intensity. Unlike gold and copper, the decay of the fronts in silver devices involved backwards movement, rather than staying in place. While the

dark feature at the anode was observed for silver, it was less pronounced compared to copper. Similarly, the brightened cathode was evident but weakest for silver. Silver devices displayed considerable outliers, including instances of previously unseen fronts and decay phenomena.

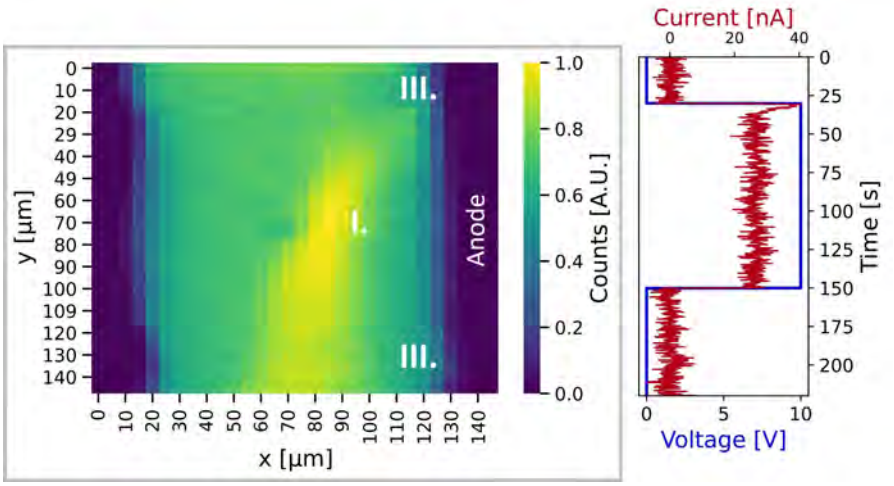

Fig. 4.12: A photoluminescence under bias map with summed and normalised intensity depicting a bright front. Applied voltage and resulting current over time are presented on the right.

Figure 4.12 depicts a PL map with a significant bright front (**I.**) emerging next to the edge of the channel. The previously present dark feature (**III.**) pushed the bright front to its side dominating the edge next to the anode - typical for the dark feature. Notably, silver devices showed a farther extent of both fronts and the dark feature compared to copper and gold. Interestingly, the front depicted here has only a slight decrease in PL signal after the bias is turned off around $y = 100\,\mu m$, whereas the front (**I.**) depicted in figure 4.5 shows an abrupt and significant decrease in overall PL signal. The current here stabilises after an initial spike, compared to the steady increase in current over time for figure 4.5. The current characteristic differs between the two but that is related to the different batches they are part of, thus likely caused by perovskite differences. Correlating the current over time to features of the ion movements is challenging though and will be discussed further in later sections.

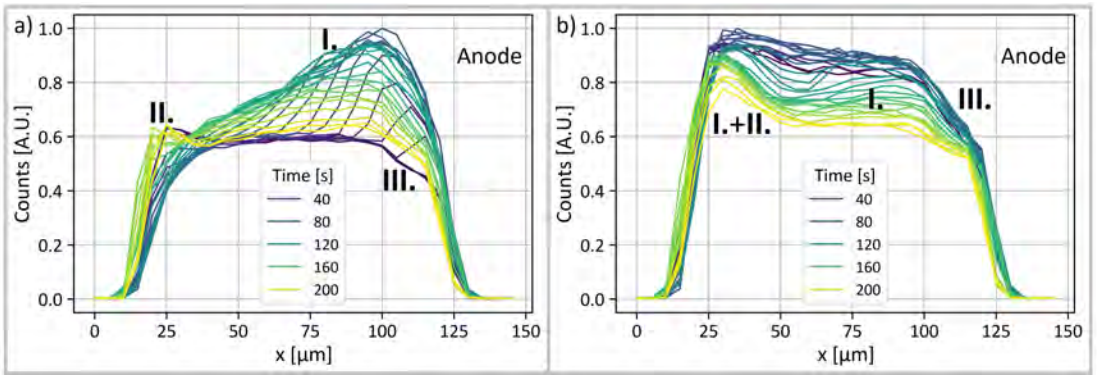

Fig. 4.13: Two photoluminescence line plots of normalised intensity (time ≡ y-axis of device channel). Map a) 10 V bias scan. Map b) subsequent 0 V unbiased scan.

Figure 4.13 depicts line plots of a 10 V biased scan and the subsequent decay scan for a silver device. The front (**I.**) is outstanding in its extent and relative intensity, nothing like any scan for copper or gold. Moreover, the decay is unique to some silver devices where the decay process separates into two distinct parts.
Looking at figure 4.13a), the initial line in purple indicates the starting condition with a slightly quenched signal at the anode (**III.**) and a brightened cathode (**II.**). Shortly after, the bias is applied, and the front (**I.**) emerges rapidly, reaching halfway across the channel within the first minute. The intensity of the front is significant, with the baseline channel signal normalised to sixty percent of the maximum intensity. Towards the end of the two-minute voltage pulse, the front nears the cathode, initiating a complicated decay process.
The cathode begins to increase in signal immediately after the voltage is no longer applied but this is not the only increase in relative signal there for long. The subsequent line plot (fig. 4.13b) shows that the decaying front moves into the same area at the cathode, entangling both processes (**I.**+**II.**). While the more intense section of the decay in figure b) plot stays close to the cathode, a dip in signal around 60 µm and 100 s indicates a split of the decaying front. The other section (**I.**) moves back towards the anode, which is typical behavior for a decaying front in silver devices. This typical part of the decay further underlines previous observations of a fast decay for fronts in silver devices as this part of the signal stabilises in a sort of ground state by the end of the scan. However, there are still clear dynamic processes at the cathode questioning that claimed observation of decay within roughly five minutes.

In summary, silver electrodes exhibited the most variance but generally showed fast, far-reaching, and intense fronts, even for low voltages. Consistent extension of fronts across the channel is not observed, as they often only reach halfway or less. However, the bright feature at the cathode was less pronounced compared to gold and copper. While a dark feature at the anode was observed, it was less intense in quenching the PL signal compared to copper. Silver devices displayed complex and varied results, presenting challenges in understanding. Nonetheless, some consistent trends emerged, which will be summarised and presented qualitatively and to some extend quantitatively in an overview table.

4.4 Overview: Metals Impact on Photoluminescence Trends

To conclude the results section, an overview table is provided with all features and key values categorised by the metals. In that way, the different features and their specific appearance for each metal is made clear.

Overview		Gold	Copper	Silver
	Work Function in [eV]	-5.1	-4.65	-4.2
Bright Front	Intensity	Lowest	High	High
	Extend (fraction of channel)	$< \frac{1}{3}$	$< \frac{1}{2}$	$\frac{1}{3}$ up to 1
	Velocity in [$\mathrm{m\,s^{-1}}$]	10^{-7}	10^{-7}	10^{-6}-10^{-7}
Bright Cathode	Intensity	High	Medium	Medium
	Occurrence	Common	Common	Less common
Dark Anode	Intensity	Low	High	Medium
I-V	Characteristic Shape (light)	Resistive	Slight S-shape	Resistive
	Max Current, OoM [nA]	Highest	Low	High
Total charge	For $10\,\mathrm{V}, 120\,\mathrm{s}$, OoM [pC]	Highest	Low	Lowest

Tab. 4.1: Overview of features and specific values categorised by the three metals gold, copper and silver. | OoM=Order of Magnitude

Table 4.1 summarises the key observations of this study. For most features, a qualitative distinction is made between the metals based on approximations. Only the work functions and the extend and velocities of the bright fronts are presented quantitatively. This is due to the severe ambiguities that come with quantifying the other features as the variance is too large and sample size too small.

The extend of the bright fronts is estimated and represents the typical front for a 10 V bias. The velocities are estimations based on the time it takes the emerging front to cover 20 µm in a PLuB map. Thus, only the order of magnitude is given which is the same for copper and silver. Silver does show significantly faster fronts but they are just between the two orders of magnitude. For each device of batches 3 and 6, I-V scans were taken before they were exposed to any other measurement. The maximum currents were averaged and based on that the ranking was made. The exact numbers are not provided, because they would falsely imply significant differences between the metals. Due to the small sample size a single outlier in one of the metals heavily impacts the average, which was the case for a gold device showing significantly higher currents. However, that is due to different channel widths that can result in higher currents. Similar to the maximum currents, the total charge, transported during a 10 V biased scan suffers from that too. Thus the same process of averaging all total charges is the basis for this ranking.

5 Discussion

The data gathered and presented in the results section encompasses different features with different appearances and complex dependencies on factors like the metal of the electrode, the bias voltage, the specific perovskite conditions and many more. To disentangle the different effects resulting in the manifold of observed phenomena requires profound analysis. In the discussion section, several proposals are advanced in an attempt to explain the observed phenomena to some extent. The proposed mechanisms aim to provide insights into the underlying physical processes. While some of these proposals are supported by experimental evidence, others have been challenged or deemed improbable. Ideas for further research are provided to validate or refine the proposed mechanisms and gain a more comprehensive understanding of the underlying dynamics.

5.1 Bright Fronts: Ions Modulating the Field Gradient?

The increasing PL signal in the channel, emerging from the high potential anode towards the cathode, is best explained by ion migration and more specifically, by vacancy-mediated halide migration. Ion dynamics have been studied extensively and based on the time scales and the reaction to applied bias, this conclusion is reached with high confidence [12]. What is unclear however, is the exact mechanism, or probably the combination of different mechanisms, facilitating increases in PL signal in the bright front. Before discussing possible mechanism, it is instructive to take into account the combined observations of this study, the previous master thesis of F. Ravazzolo [21] and unpublished work by J. Thiesbrummel where bright fronts were observed. Interestingly, whereas in this study an electron selective layer was used, they used a hole selective layer and no charge transport layer at all, respectively. Thus, the observed bright front feature is most likely a perovskite intrinsic process and not caused by other layers. Still, the architecture, layers, materials, and perovskite composition may significantly influence the processes at hand. Regardless, it holds that explanations of the bright front can not be reduced to interactions with e.g. the C60 layer.
Different proposed mechanisms come with their own specific merits and drawbacks but so far, no single one can be clearly determined to be the cause for the observed bright fronts. A first approach looks at the migrating halide vacancies being the direct cause for the increased PL signal at the anode: With applied bias, the effectively positively charged vacancies are pushed away from the anode leaving behind a vacancy-poor perovskite with decreased trap density ultimately resulting in increased radiative recombination [20]. This immediately poses the question why there is no decrease in PL intensity near

the cathode. If the vacancies were to cause non-radiative recombination, then moving them towards the cathode should result in quenched PL in that part of the channel which was never observed. Thus, this is not likely the only mechanism explaining the gathered data.
Similarly, it might be the case that halide interstitials filling vacancies are responsible for the increased signal. But the observed decay trends are hard to explain that way. Filled vacancies are not expected to re-emerge after the bias has been released because that would require them to escape an energetically favoured state without bias.

A simple and general explanation may be found in the electric field distribution across the channel, similar to what was proposed by Li et al. [43]. Ions are known to influence the electric field distribution [12] but the specific distributions are hard to determine. The potential gradient determines the dynamics of electrical charge carriers, where high gradients force charges to drift and flat potentials do not enact force upon them. Thus, a specific constellation of accumulated ions could result in an extended field-free region, hindering charge extraction from that region. In that way, an increase in radiative recombination could be caused by mobile ions in just the way it was observed in different scenarios. So, as soon as the bias is applied across the channel, halide vacancies may be pushed away from the anode resulting in an effective accumulation of halides close to the anode. The accumulated ionic charges may partially screen the electrical field causing a reduction of the gradient and thus, may reduce the drive of electronic carriers to leave the area. With the potentially increased electrical carrier density, increased radiative recombination and with that higher intensity PL follow naturally resulting in the appearance of an extending brightened PL area. The effect would decrease for higher distances to the interface resulting in locally limited fronts. After the bias is turned off, the accumulated ions may dissipate slowly recovering the ground state. This would also allow for the differences in appearance for the metals, as the energy alignment may very well allow for specific differences in potential gradient due to changes in ion accumulation.
Depending on the specific conditions, the resulting effects from ion modulated field gradient may differ significantly, explaining different observations such as bright or dark fronts. In some cases, the field screening may not allow for improved radiative recombination or other effects dominate it. However, as a broad concept this explanation is versatile and holds intuitive explanatory power. Simulations are suitable to investigate whether such a mechanism could reproduce a similar increase in radiative recombination. If so, the hypothesis gains validity and may be further investigated.

A different but related approach is centered around changes in energy levels and the occupation of trap states, influenced by migrating ions. Due to the migration of ions, the energy levels of the perovskite crystal are changed locally, which may cause previously empty trap states to be permanently filled. In that way, an increase in radiative recombination would be facilitated by migrating ions in a reversible way, nicely aligning with the observed features.
The same mechanism could also cause previously filled trap states to empty and become available for non-radiative recombination resulting in quenched PL signal and the emergence of dark fronts. In combination with the previously proposed mechanism, the presence of those traps in the region where accumulated ions screen the field could possibly lead to dark instead of Bright fronts. Thereby, this mechanism could explain both bright and dark fronts, depending on the exact conditions of the perovskite, its composition, and exterior circumstances. However, this hypothesis is not backed by simulations or computations showing feasible changes in trap state occupation and the ions influence on them. Thus, for now, it remains a hypothesis that is neither refuted nor underlined, and which could be further investigated (e.g. PL lifetime).

Aside from short term investigation using simulations, further experimental research would certainly provide crucial insight, as specific influences could be investigated in more detail. For example, testing different compositions could highlight the impact of specific ions or their concentrations. Firstly, employing over or understoichiometric amounts of halides or cations, and studying their impact on the bright fronts allows to gain insight into which species are responsible. Of course, employing different perovskite composition would be interesting as compositional changes certainly impact the processes, e.g. studying the prototypical $MAPbI_3$ allows for a broad pool of comparisons as this composition has been thoroughly studied [19]. Moreover, changing the charge selective layer provides further insight into the role the C60 plays in the observed features, as it seems to not have a big impact. However, it might be the case that the previously not observed bright feature at the cathode could be related to a C60 interactions, as PLuB is usually conducted without an ETL/C60. Employing metals with similar work functions to those tested (e.g. Al for AG and Cr for Cu) would help disentangle the effect of the metals work function from other properties like reactivity or more complicated interactions.
Utilising complementary measurement methods would provide additional insight. During this project, attempts were made to relate dynamics in bias assisted charge extraction (BACE) measurements to dynamics in the PL maps. A BACE measurement is conducted

every time a biased PL scan is measured as BACE entails applying a voltage pulse and investigating the current dynamics during and after the pulse. However, interpretation of the gathered data is challenging and due to a lack of time, it is not a part of this report. Still, insights are to be gained from this method as decay time constants or dynamics during applied voltage can be studied and modelled.
Another potentially insightful method uses scanning Kelvin probe force microscopy (KPFM) to study the electrical field [44]. KPFM measures the surface potential of a conductive sample and examination of these lateral perovskite devices could provide insights into the potential distribution and accumulation of charges in the perovskite channel. At last we suggest impedance spectroscopy for these lateral perovskite devices as it provides time constants for mobile charges, which could then be related to the processes observed in the PLuB maps.

In summary, the remarkable bright front feature consistently observed in this research project can not be explained conclusively. However, a likely and general explanation is related to changes in field gradient caused by accumulated halide ions. A reduced field gradient near the anode could lead to higher electrical charge carrier densities resulting in increases in overall photoluminescence intensity. The metal may impact the potential gradient and therefore the accumulation of ions, therefore modulating but not fundamentally changing the mechanism of bright fronts.

5.2 Dark Feature: Migration, Degradation or Metal Impurities?

Whereas the previously discussed bright front feature displays dynamic increases in PL signal, the second feature to be discussed is quenching occurring over longer time scales. This feature is more comparable to the many other findings of PLuB measurements reported in literature, as the quenching of the PL signal on a minute time scale has been widely reported [19].
This feature appeared only after a bias has been applied multiple times and emerged slowly throughout bias applications. Compared to the faster bright fronts, this feature may be related to the migration of another species or a different mechanism altogether. The reduction in overall PL signal implies reduction of radiative- and an increase in non-radiative recombination rates in the perovskite. A simplified explanation may be suggested where the migration of ion defects, as in vacancies, migrate away from the anode leaving behind non-radiative and PL quenching sites [19].
Another correlation has been established by Birkhold et al. where a similar device is employed and studied using PLuB and KPFM. They show that introducing an insulator

layer still allows for ion migration but no according dark front is seen in that case, compared to the dark front they observe for devices without an insulating layer (perovskite in direct contact with gold). They propose the front (notably, in their case the front emerges from the cathode rather than the anode) is caused by interplay of mobile ions and injection of electronic carriers from the (in that cased not insulated) electrodes [44]. Further, it is proposed that Pb defects, specifically the uncharged Pb_i^0 interstitials, form deep trap states, being responsible for the non-radiative recombination and quenched PL signal. However, in that case $MAPbI_3$ was used, whereas $FAPbI_3$ did not show any dark front possibly due to the lower trap level calculated by them. Following from that, and looking at the formamidinium dominated perovskite composition, it is unlikely that the reduction of Pb_i^{2+} to Pb_i^0 and the subsequently enhanced non-radiative recombination is causing the dark feature observed in this study. However, changes in composition and or other factors in this study may cause the calculated trap levels to be different from the actual ones. Thus, this mechanism can not be excluded easily and remains a possibility.
A different mechanism related to metal impurities could also be proposed to explain the quenched signal at the anode. If positively charged metal impurities may migrate into the perovskite [23][24], a related increase in non-radiative recombination is imaginable. The slow appearance and negligible decay within a measurement session could be explained by an energy barrier for the metal impurities, only overcome by a combination of (laser) light and bias. The problem of different metals causing the same mechanism is not that unlikely here, as metal impurities of any of the electrode metals could react with the perovskite, causing deep trap states. This could also explain the lack of decay of this feature, as those reactions may not be reversible. However, a study by Ming et al. claims that out of copper, gold and silver, only migrated gold impurities form deep trap states causing quenched PL signal [24]. If that is the case, the dark features observed for devices of all metals cannot be explained by migrated metal impurities as silver and copper should not form deep trap states. However, if the metal impurities indirectly cause the quenching by reacting with the perovskite, the proposition still holds.
Thus, a proper explanation could not be presented here, but further research should provide answers and confirmations on a short time scale. Firstly, a more dedicated study of this specific feature should clear up questions of reversibility or decay of this feature, by measuring a device multiple times in e.g. hourly intervals after the feature has emerged. Also, looking into the effect of opposite bias on this feature may also provide insights into reversibility and potential carrier dynamics at hand. Further, changes in the architecture are always insightful, as changing the ETL material, replacing it with an HTL or even an insulating layer could provide further insight into the specifics of this dark

feature. By employing other measurement methods a combination of data could clear up the relation between the metal and the dark front. For example, X-ray fluorescence measurements could underline or overrule the metal impurity related explanation as varying metal concentrations inside the channel would be related to PL features.
This feature remains unclear, however, it shares a lot of similarities with previously reported dark fronts. Possibly, Pb_i^0 or positively metal electrode impurities inside the channel could cause the PL quenching on longer time scales.

5.3 Cathode Light Up: Chemical Reactions are likely Candidate

A curious feature is the increased signal at the cathode, emerging only after a device has already been exposed to applied bias, similar to how the dark feature appears. Here too, the signal increases in relative intensity throughout a measuring session but interestingly, during applied bias, this signal disappears. Due to voltage seemingly being necessary in order for this feature to appear, but its disappearance during bias, ion dynamics do not seem to fit. If accumulated ions at the cathode were to explain this brightening, why would it be quenched during applied bias, the driving force of ion accumulation? Thus, another mechanism might be required to explain the increased signal at the cathode.
Regarding the double halide perovskite used during this project, halide segregation comes to mind as a candidate to explain the increased signal. In the aforementioned fundamental paper of Hoke et al. they investigate mixed iodine bromine perovskites and their reaction to light soaking using PL and XRD [22]. It is found that halide segregated phases occur with improved PL yield in the short term, related to light soaking effects, whereas, on a longer term, they might cause severe degradation decreasing performance. However, the 6 % bromine concentration employed in this study does not usually show the occurrence of this Hoke effect as concentrations of 20 % or higher are required for that [9]. Moreover, with segregated phases, spectral changes in the PL signal are expected due to carriers funneling into the iodide-dominated lower bandgap regions but none are observed. Thus, this explanation suffers from drawbacks questioning its validity.

Another candidate to explain the observed feature does not involve ion migration directly, as it rather focuses on potential chemical reactions at the interface.
Chemical reactions fit the observed behaviours, especially concerning bias, as they have to be started by a certain threshold energy, being provided by the applied bias. But when the chemical reactions have started and the device is left in the dark, the effect actually intensifies, possibly related to more reactions taking place. With the complex composition of elements and molecules at the interface between the double cation double

halide perovskite, the C60 and BCP transport layer, and the metal electrode, a multitude of chemical reactions are possible. Thus, chemical reactions could occur passivating the surface and resulting in limited non-radiative recombination and increased PL signal. The fact that an increse in PL intensity is not seen during bias could be explained by very efficient extraction of carriers close to the cathode Or it might be the case that the chemical reactions create a potential well near the reaction site attracts charge carriers causing the increased PL signal when no bias is applied. Then, during applied bias, the field gradient across the channel dominates the small potential well near the cathode extracting the surplus of carriers that caused the increased signal. After the bias is turned off again, the wells are attracting carriers again and the PL intensity increases again.
Finally, it is interesting to mention that gold was the metal most prominently showing this feature and it is the metal related to severe chemical reactions at the interface [23]. However, this would usually go along with increased non-radiative recombination and thus the opposite of what is observed here.
A drawback to this explanation is a the lack of a spectral peak shift which would be expected if chemical reactions take place in a significant amount. Analysing the peak position in PL maps depicting this bright feature does not show any shift in the emitted spectrum. The missing peak shift questions the validity but does not necessarily disprove the suggested mechanism.

Studying similar device architectures should provide further insights as changing charge transport layers and materials would change the chemical landscape possibly influencing the feature. Another interesting way to check the mechanism that involves passivating chemical reactions would be to use passivated surfaces to start with. Implementing the molecule trioctylphosphine oxide (TOPO) can passivate perovskite surfaces rendering it an interesting approach to investigate the proposed mechanism [45].
Thus, for this feature too, a comprehensive analysis could not be provided. Chemical reactions somehow related to passivating surface sites seem to be a likely candidate in causing this feature. Becasue this feature was not obbserved previously, it might be correlated to the C60 layer. This is proposed because of the similarities between the devices and according features studied here and the ones studied by F. Ravazzolo that did not show this specific trend and the main difference is C60 compared to NiO.

5.4 The Metals Impact: More than just the Work Function?

The research question of this study deals with the impact that metals have on the ion dynamics within a perovskite device. Because of the multitude of factors and mechanisms at play, forming an entangled and hard to discern set of interactions, providing a comprehensive answer is challenging. Still, consistent difference were established between the metals, all showing the same features but with significant changes in their appearance. Thus, it can be concluded that metals certainly have an influence on ion dynamics. However, the question remains to what extend and in which way they do.
A difference in work function is the most basic distinction between the metals related to the ion migration and accumulation processes. With different energy levels and alignments comes a difference in electrical field distribution across the channel and especially close to the interfaces. Thus, the same perovskite intrinsic feature might be changed by different metals as the features heavily depend on local field gradient. Varied extend and intensity of a given feature could be explained by the differences of the field gradient.
For further study, employing metals with similar work functions would provide insights into whether the work function is the main cause for to the observed differences. Studying devices with Cr and Al electrodes is thus the suggested next step. In order to investigate if migrated metal impurities play a role, either employing measurement techniques to investigate metal presence in the channel, or utilising a high diffusion barrier metal, are potential directions of research. And finally, investigating the chemical reactions taking place near the interfaces and the metals impact on them is an interesting but also challenging path to take further research.

It is likely the case that the work function does play a significant role in ion dynamics as the energy alignment between metal and perovskite modulates the field distribution in the device. However, the gathered data implies that more factors contribute to the observed phenomena.

Conclusion

In conclusion, this study delved into the influence of metal electrodes on ion dynamics through the lens of electrically biased photoluminescence microscopy. A thorough examination of each observed feature was conducted, analysing the impact of different metals and proposing mechanistic explanations.
A notable discovery among the features are the bright fronts characterised by increased luminescence intensity emerging near the anode. These fronts, scarcely reported in literature, are theorised to stem from ion-induced modulations of the electrical field, resulting in localised increases in charge density and subsequent enhancements in radiative recombination rates. Alternatively, migrating ions may suppress non-radiative recombination by modulating band energies and occupation of trap states.
It is evident that copper, gold, and silver electrodes manifest similar features, albeit with notable variations in appearance. Silver devices, potentially due to energy alignment, exhibit intense bright fronts characterised by higher speed and extended reach across the channel when compared to those with gold or copper electrodes. Additionally, two other features are identified: a dark front at the anode on longer timescales and an increase in luminescence intensity at the cathode. These features are more pronounced and prevalent for copper and gold electrodes, respectively.

Overall, the findings contribute to a deeper understanding of the intricate relationship between metal electrodes and ion migration in metal halide perovskites, offering valuable insights for the development of future photovoltaic and optoelectronic devices. Further research is warranted to clarify the underlying mechanisms driving these phenomena and to explore their potential implications for device performance and stability.

References

[1] Core Writing Team, H. Lee and J. Romero (eds.): *Climate Change 2023: Synthesis Report. Contribution of Working Groups I, II and III to the Sixth Assessment Report of the Intergovernmental Panel on Climate Change*. IPCC, Geneva, Switzerland, 2023.

[2] *World gross electricity production by source*. IEA, Paris, France, 2019.

[3] Ritchie, Hannah and Pablo Rosado: *Energy mix*. Our World in Data, 2020. https://ourworldindata.org/energy-mix.

[4] Ballif, Christophe, Franz Josef Haug, Mathieu Boccard, Pierre J. Verlinden, and Giso Hahn: *Status and perspectives of crystalline silicon photovoltaics in research and industry*. Nature Reviews Materials, 7(8):597–616, August 2022, ISSN 2058-8437.

[5] Kojima, Akihiro, Kenjiro Teshima, Yasuo Shirai, and Tsutomu Miyasaka: *Organometal halide perovskites as visible-light sensitizers for photovoltaic cells*. Journal of the American Chemical Society, 131(17):6050–6051, May 2009, ISSN 0002-7863, 1520-5126.

[6] Bati, Abdulaziz S. R., Yu Lin Zhong, Paul L. Burn, Mohammad Khaja Nazeeruddin, Paul E. Shaw, and Munkhbayar Batmunkh: *Next-generation applications for integrated perovskite solar cells*. Communications Materials, 4(1):2, January 2023, ISSN 2662-4443.

[7] Schmidt-Mende, Lukas and Jonas Weickert: *Organic and Hybrid Solar Cells*. De Gruyter, Paris, 1st edition, 2016, ISBN 978-3-11-028318-1.

[8] McGovern, Lucie, Esther Alarcón-Lladó, Erik C. Garnett, Bruno Ehrler, and Bob Van Der Zwaan: *Perovskite solar modules for the residential sector*. ACS Energy Letters, 8(11):4862–4866, November 2023, ISSN 2380-8195, 2380-8195.

[9] Boyd, Caleb C., Rongrong Cheacharoen, Tomas Leijtens, and Michael D. McGehee: *Understanding degradation mechanisms and improving stability of perovskite photovoltaics*. Chemical Reviews, 119(5):3418–3451, March 2019, ISSN 0009-2665, 1520-6890.

[10] Wikipedia contributors: *Perovskite (structure) — Wikipedia, the free encyclopedia*, 2024. `https://en.wikipedia.org/w/index.php?title=Perovskite_(structure)&oldid=1207466600`, [Online; accessed 24-February-2024].

[11] Goetz, Katelyn P., Alexander D. Taylor, Fabian Paulus, and Yana Vaynzof: *Shining light on the photoluminescence properties of metal halide perovskites.* Advanced Functional Materials, 30(23):1910004, June 2020, ISSN 1616-301X, 1616-3028.

[12] Zuo, Lijian, Zexin Li, and Hongzheng Chen: *Ion migration and accumulation in halide perovskite solar cells †.* Chinese Journal of Chemistry, 41(7):861–876, April 2023, ISSN 1001-604X, 1614-7065.

[13] An, Yu, Carlo Andrea Riccardo Perini, Juanita Hidalgo, Andrés Felipe Castro-Méndez, Jacob N. Vagott, Ruipeng Li, Wissam A. Saidi, Shirong Wang, Xianggao Li, and Juan Pablo Correa-Baena: *Identifying high-performance and durable methylammonium-free lead halide perovskites via high-throughput synthesis and characterization.* Energy & Environmental Science, 14(12):6638–6654, 2021, ISSN 1754-5692, 1754-5706.

[14] Zarick, Holly F., Naiya Soetan, William R. Erwin, and Rizia Bardhan: *Mixed halide hybrid perovskites: a paradigm shift in photovoltaics.* Journal of Materials Chemistry A, 6(14):5507–5537, 2018, ISSN 2050-7488, 2050-7496.

[15] Bi, Enbing, Zhaoning Song, Chongwen Li, Zhifang Wu, and Yanfa Yan: *Mitigating ion migration in perovskite solar cells.* Trends in Chemistry, 3(7):575–588, 2021, ISSN 2589-5974.

[16] Tress, Wolfgang: *Metal halide perovskites as mixed electronic–ionic conductors: Challenges and opportunities—from hysteresis to memristivity.* The Journal of Physical Chemistry Letters, 8(13):3106–3114, July 2017, ISSN 1948-7185, 1948-7185.

[17] Eames, Christopher, Jarvist M. Frost, Piers R. F. Barnes, Brian C. O'Regan, Aron Walsh, and M. Saiful Islam: *Ionic transport in hybrid lead iodide perovskite solar cells.* Nature Communications, 6(1):7497, June 2015, ISSN 2041-1723.

[18] Shao, Yuchuan, Yanjun Fang, Tao Li, Qi Wang, Qingfeng Dong, Yehao Deng, Yongbo Yuan, Haotong Wei, Meiyu Wang, Alexei Gruverman, Jeffery Shield, and Jinsong Huang: *Grain boundary dominated ion migration in polycrystalline*

organic–inorganic halide perovskite films. Energy & Environmental Science, 9(5):1752–1759, 2016, ISSN 1754-5692, 1754-5706.

[19] Zhang, Jing, Cheng Li, Mengyu Chen, and Kai Huang: *Real-time observation of ion migration in halide perovskite by photoluminescence imaging microscopy.* Journal of Physics D: Applied Physics, 54(4):044002, January 2021, ISSN 0022-3727, 1361-6463.

[20] Luo, Yanqi, Parisa Khoram, Sarah Brittman, Zhuoying Zhu, Barry Lai, Shyue Ping Ong, Erik C. Garnett, and David P. Fenning: *Direct observation of halide migration and its effect on the photoluminescence of methylammonium lead bromide perovskite single crystals.* Advanced Materials, 29(43):1703451, November 2017, ISSN 0935-9648, 1521-4095.

[21] Ravazzolo, Federico: *Ionic-electronic interplay in perovskites*, 2023. `https://amolf.nl/research-groups/hybrid-solar-cells/publications`.

[22] Hoke, Eric T., Daniel J. Slotcavage, Emma R. Dohner, Andrea R. Bowring, Hemamala I. Karunadasa, and Michael D. McGehee: *Reversible photo-induced trap formation in mixed-halide hybrid perovskites for photovoltaics.* Chemical Science, 6(1):613–617, 2015, ISSN 2041-6520, 2041-6539.

[23] Lin, Chun-Ho, Long Hu, Xinwei Guan, Jiyun Kim, Chien-Yu Huang, Jing-Kai Huang, Simrjit Singh, and Tom Wu: *Electrode engineering in halide perovskite electronics: Plenty of room at the interfaces.* Advanced Materials, 34(18):2108616, May 2022, ISSN 0935-9648, 1521-4095.

[24] Ming, Wenmei, Dongwen Yang, Tianshu Li, Lijun Zhang, and Mao-Hua Du: *Formation and diffusion of metal impurities in perovskite solar cell material CH3NH3PbI3: Implications on solar cell degradation and choice of electrode.* Advanced Science, 5(2):1700662, February 2018, ISSN 2198-3844, 2198-3844.

[25] Domanski, Konrad, Juan Pablo Correa-Baena, Nicolas Mine, Mohammad Khaja Nazeeruddin, Antonio Abate, Michael Saliba, Wolfgang Tress, Anders Hagfeldt, and Michael Grätzel: *Not all that glitters is gold: Metal-migration-induced degradation in perovskite solar cells.* ACS Nano, 10(6):6306–6314, June 2016, ISSN 1936-0851, 1936-086X.

[26] McMeekin, David P., Golnaz Sadoughi, Waqaas Rehman, Giles E. Eperon, Michael Saliba, Maximilian T. Hörantner, Amir Haghighirad, Nobuya Sakai, Lars Korte, Bernd Rech, Michael B. Johnston, Laura M. Herz, and Henry J. Snaith: *A*

mixed-cation lead mixed-halide perovskite absorber for tandem solar cells. Science, 351(6269):151–155, January 2016, ISSN 0036-8075, 1095-9203.

[27] Akhil, S., S. Akash, Altaf Pasha, Bhakti Kulkarni, Mohammed Jalalah, Mabkhoot Alsaiari, Farid A. Harraz, and R Geetha Balakrishna: *Review on perovskite silicon tandem solar cells: Status and prospects 2t, 3t and 4t for real world conditions.* Materials & Design, 211:110138, December 2021, ISSN 02641275.

[28] Gu, Shuai, Renxing Lin, Qiaolei Han, Yuan Gao, Hairen Tan, and Jia Zhu: *Tin and mixed lead–tin halide perovskite solar cells: Progress and their application in tandem solar cells.* Advanced Materials, 32(27):1907392, July 2020, ISSN 0935-9648, 1521-4095.

[29] Wojciechowski, Konrad, Tomas Leijtens, Svetlana Siprova, Christoph Schlueter, Maximilian T. Hörantner, Jacob Tse Wei Wang, Chang Zhi Li, Alex K. Y. Jen, Tien Lin Lee, and Henry J. Snaith: *C 60 as an efficient n-type compact layer in perovskite solar cells.* The Journal of Physical Chemistry Letters, 6(12):2399–2405, June 2015, ISSN 1948-7185, 1948-7185.

[30] Lee, Hyun Jung and Seok In Na: *Investigation of pcbm/zno and c60/bcp-based electron transport layer for high-performance p-i-n perovskite solar cells.* Journal of Alloys and Compounds, 921:166007, November 2022, ISSN 09258388.

[31] Liu, Dianyi, Qiong Wang, Christopher J. Traverse, Chenchen Yang, Margaret Young, Padmanaban S. Kuttipillai, Sophia Y. Lunt, Thomas W. Hamann, and Richard R. Lunt: *Impact of ultrathin c 60 on perovskite photovoltaic devices.* ACS Nano, 12(1):876–883, January 2018, ISSN 1936-0851, 1936-086X.

[32] Coskun, Hikmet, Furkan H. Isikgor, Zhihui Chen, Muhammad Imran, Bichen Li, Qinghua Xu, and Jianyong Ouyang: *Thermally evaporated two-dimensional sns as an efficient and stable electron collection interlayer for inverted planar perovskite solar cells.* Journal of Materials Chemistry A, 7(9):4759–4765, 2019, ISSN 2050-7488, 2050-7496.

[33] Heidel, T. D., D. Hochbaum, J. M. Sussman, V. Singh, M. E. Bahlke, I. Hiromi, J. Lee, and M. A. Baldo: *Reducing recombination losses in planar organic photovoltaic cells using multiple step charge separation.* Journal of Applied Physics, 109(10):104502, May 2011, ISSN 0021-8979.

[34] Prathapani, Sateesh, Parag Bhargava, and Sudhanshu Mallick: *Electronic band structure and carrier concentration of formamidinium–cesium mixed cation lead mixed halide hybrid perovskites.* Applied Physics Letters, 112(9):092104, February 2018, ISSN 0003-6951.

[35] Srivastava, Vaibhava, R. K. Chauhan, Pooja Lohia, and Shivangi Yadav: *Achieving above 25 % efficiency from fa0.85cs0.15pb(i0.85br0.15)3 perovskite solar cell through harnessing the potential of absorber and charge transport layers.* Micro and Nanostructures, 184:207691, 2023, ISSN 2773-0123.

[36] Instruments, Edinburgh: *What is confocal raman microscopy?* `https://www.edinst.com/us/blog/what-is-confocal-raman-microscopy/`.

[37] Tan, Wen Liang and Christopher R. McNeill: *X-ray diffraction of photovoltaic perovskites: Principles and applications.* Applied Physics Reviews, 9(2):021310, May 2022, ISSN 1931-9401.

[38] Sciprios: *Spinbot: A fully automated, customizable spin-coating robot.* `https://www.sciprios.de/lab-automation/spincoating-robots/`.

[39] Wikipedia contributors: *Electrical discharge machining — Wikipedia, the free encyclopedia*, 2024. `https://en.wikipedia.org/w/index.php?title=Electrical_discharge_machining&oldid=1210418887`, [Online; accessed 29-February-2024].

[40] Ven, Anton Van der, Kimberly A. See, and Laurent Pilon: *Hysteresis in electrochemical systems.* Battery Energy, 1(2):20210017, 2022. `https://onlinelibrary.wiley.com/doi/abs/10.1002/bte2.20210017`.

[41] Mörée, Gustav and Mats Leijon: *Review of hysteresis models for magnetic materials.* Energies, 16:3908, May 2023.

[42] Lin, Lu, Li Yang, Guozheng Du, Xiaofeng Li, Ya nan Li, Jidong Deng, Kun Wei, and Jinbao Zhang: *Light soaking effects in perovskite solar cells: Mechanism, impacts, and elimination.* ACS Applied Energy Materials, 6(20):10303–10318, 2023.

[43] Li, Cheng, Antonio Guerrero, Sven Huettner, and Juan Bisquert: *Unravelling the role of vacancies in lead halide perovskite through electrical switching of photoluminescence.* Nature Communications, 9(1):5113, November 2018, ISSN 2041-1723.

[44] Birkhold, Susanne T., Jake T. Precht, Hongbin Liu, Rajiv Giridharagopal, Giles E. Eperon, Lukas Schmidt-Mende, Xiaosong Li, and David S. Ginger: *Interplay of mobile ions and injected carriers creates recombination centers in metal*

halide perovskites under bias. ACS Energy Letters, 3(6):1279–1286, June 2018, ISSN 2380-8195, 2380-8195.

[45] Huang, Guangguang, Chunlei Wang, Hao Zhang, Shuhong Xu, Qingyu Xu, and Yiping Cui: *Post-healing of defects: an alternative way for passivation of carbon-based mesoscopic perovskite solar cells via hydrophobic ligand coordination.* Journal of Materials Chemistry A, 6(6):2449–2455, 2018, ISSN 2050-7488, 2050-7496.

List of Figures

List of Tables